Neuregulin1 regulates cardiomyocyte dynamics, proliferation, and maturation during ventricular chamber morphogenesis

Joaquim Grego-Bessa[1,2], Paula Gómez-Apiñaniz[1,2], Belén Prados[1,2], Manuel José Gómez[3], Donal MacGrogan[1,2,*] & José Luis de la Pompa[1,2,*]

Centro Nacional de Investigaciones Cardiovasculares Carlos III (CNIC), Melchor Fernández Almagro 3, 28029 Madrid, SPAIN.

[2] CIBER de Enfermedades Cardiovasculares, Madrid, SPAIN

[3] Bioinformatics Unit, CNIC, Madrid SPAIN

[*] Corresponding authors: dmacgrogan@cnic.es, jlpompa@cnic.es. Phone: +34-620-936633

BACKGROUND: Cardiac ventricles are essential for providing the contractile force of the beating heart throughout life. How the primitive endocardium-layered myocardial projections called trabeculae form and mature into the adult ventricles is of great interest for fundamental biology and regenerative medicine. Trabeculation is dependent on the signaling protein Neuregulin1 (NRG1). However, the mechanism of action of NRG1 and its role in ventricular wall maturation are poorly understood.

METHODS: The function and downstream mechanisms of NRG1 signaling during ventricular chamber development were explored in mice with conditional cardiac-specific-*Nrg1* depletion or overexpression using confocal imaging, transcriptomics, and biochemical approaches.

RESULTS: Analysis of cardiac-specific-*Nrg1* mutant mice showed that the apicobasal polarity transcriptional program underlying cardiomyocyte-oriented cell division and trabeculae formation depends on endocardial NRG1 to myocardial ERBB2 signaling and pERK activation. Early endothelial loss of NRG1 reduced cardiomyocyte PAR3 expression and apical-domain expression of CRUMBS, caused N-CADHERIN mis-localization, and altered actin cytoskeletal organization. Impaired trabeculation in *Nrg1* mutants was associated with a directional shift from perpendicular to parallel/obliquely-oriented cardiomyocyte division. Later endothelial NRG1 depletion resulted in ventricular hypoplasia and lack of an inner compact myocardial wall. Gene profiling indicated that NRG1 is required for trabecular growth and ventricular wall thickening by regulating an epithelial-to-mesenchyme transition (EMT)-like process in cardiomyocytes involving migration, adhesion, cytoskeletal actin turnover, and timely progression through the cell cycle. Cardiac NRG1 overexpression and pERK hyperactivation maintained high EMT-like gene expression and prolonged the trabeculation phase, hindering the formation and maturation of the compact myocardial wall. Likewise, alterations to myocardial trabecular patterning resulting from above- or below-normal NRG1 expression were concomitant with profound disorganization of the sarcomere actin cytoskeleton. The NRG1 loss- and gain-of-function transcriptomes were enriched for an EMT-like gene signature associated with yes-associated protein-1 (YAP1), identifying YAP1 as a potential downstream effector. Biochemical and imaging data showed that pERK activation and nuclear-cytoplasmic distribution of YAP1 during trabeculation are dependent on NRG1.

CONCLUSIONS: These data establish NRG1 as a crucial orchestrator of cardiomyocyte proliferation and migration during ventricular development and identify a NRG1-dependent signaling cascade that could be leveraged for future cardiac regenerative therapies.

Key Words: Ventricular development, trabeculation, oriented cell division, compaction, ventricular conduction system, actin cytoskeleton, EMT-like, A-B polarity, NRG1, ERBB2, YAP1.

Nonstandard Abbreviations and Acronyms

4OH-TAM, 4-hydroxytamoxifen

A-B polarity, apico basal polarity

CM, compact myocardium

EMT-like, epithelial-mesenchymal transition-like

ERBB2/4, erb-b2 receptor tyrosine kinase 2/4

ERK, extracellular signal regulated MAP kinase

GOF, gain-of-function

GSEA, gene set enrichment analysis

IF, immunofluorescence

LOF, loss-of-function

NRG1, neuregulin1

OCD, oriented cell division

OE, overexpression

SMA, smooth muscle actin

SM22, smooth muscle cell-specific cytoskeletal protein

TM, trabecular myocardium

VCS, ventricular conduction system

YAP1, yes1-associated transcriptional regulator

Novelty and Significance

WHAT IS KNOWN?

- Myocardial trabeculae are required for ventricular chamber growth, development of the conduction system, and the formation of the coronary arteries.
- Trabeculae are initiated by oriented cell division (OCD), and trabecular growth is driven by directional migration.
- The membrane glycoprotein neuregulin1 (NRG1) mediates cell-cell signaling and is essential for trabecular development.

WHAT NEW INFORMATION DOES THIS ARTICLE CONTRIBUTE?

- NRG1 signaling is required for apicobasal cardiomyocyte polarity and cytoskeletal organization during the oriented cell division underlying trabeculation.
- NRG1 is required for the formation of the inner ventricular wall but not the coronaries.
- NRG1 regulates motility and cell-cycle progression during ventricular wall growth.
- Ectopic NRG1 expression trabeculates myocardium and arrests cardiac development.
- NRG1 regulates ventricular patterning mediated by cytoskeletal dynamics and modulates pERK-dependent YAP1 S274 phosphorylation during trabeculation.
- NRG1 is not required for ventricular compaction.

Introduction

Ventricular chamber development entails transient morphogenetic changes that include the formation of trabeculae, their expansion and growth, and their subsequent incorporation into a compact muscular wall. Fate-mapping and time-lapse live imaging in zebrafish has shown that trabeculae form by the extrusion of cardiomyocytes and their radial extension along the inner curvature of the looping heart and into the ventricular lumen [1-5]. In mice, trabeculation begins with oriented cell division (OCD) perpendicular to the ventricular inner wall plane, and trabecular growth is driven by directional migration from the outer (epicardial) layer toward the inner (endocardial) layers [6-8]. The process of trabeculae coalescence forms a dense meshwork that maximizes ventricular surface area for nutrient and gas exchange in the absence of a coronary circulation [9]. This meshwork later differentiates into a specialized ventricular conduction system and is resolved by expansion of the compact myocardial wall, with trapped endocardial cells giving rise to the coronary arteries [10-14].

Trabeculation defects or failed compaction in humans manifests as hypertrabeculation or non-compaction phenotypes [15]. Trabeculae thickening, decreased intertrabecular spacing, and underdevelopment of the compact wall myocardium are defining morphological features of left ventricular non-compaction cardiomyopathy [16]. This phenotype is a feature of several conditions, for which links have been identified with sarcomeric genes and cardiac contractility, calcium handling, and developmental signaling pathways [17]. Conversely, acquired non-compaction or the appearance of hypertrabeculation in trained athletes or during pregnancy, have been interpreted as morphophysiological manifestations of increased hemodynamic load [18]. Moreover, genetic association and Mendelian randomization studies have found an inverse relationship between the complexity of trabecular morphology and the risk of cardiovascular disease, pointing to a potentially beneficial role of excessive trabeculation in adults [19]. Given the diversity of underlying pathophysiological mechanisms, there is ongoing debate about the significance of hypertrabeculation and non-compaction within the spectrum of myocardial adaptive processes and diseases [18, 20-22].

Trabecular development requires the intercellular signaling action of the membrane glycoprotein neuregulin1 (NRG1) [4, 23-25]. This endocardial protein directly binds to epidermal growth factor receptor tyrosine kinase (ERBB4) on adjacent cardiomyocytes, triggering ERBB2 ligand-stimulated heterodimerization and tyrosine phosphorylation, followed by activation of downstream pathways [26], including the phopho-extracellular signal-regulated kinase (pERK) intracellular signaling pathway [27]. Targeted mutation of *Erbb2* or *nrg2a* in fish [3, 4, 25], or deletion of *Nrg1*, *ErbB2*, or *ErbB4* in mice [24, 28-32], blocks trabeculation. Cardiomyocyte proliferation and contractility, which are required for trabeculation, are impaired in mutant *ErbB4* mice [33] and *erbb2* zebrafish [3], whereas potentiation of ErbB2 signaling in mouse adult cardiomyocytes promotes proliferation and myocardial regeneration [34]. Consistent with these findings, beneficial effects of NRG1 for cardiac function have

been reported in mouse models of cardiac injury [33]; explanted human tissue [35]; ischemic, dilated, and viral cardiomyopathy [36]; and heart failure [37-39]. Clinical trials with different forms of recombinant NRG1 support a cardioprotective role in systolic heart failure [40], although the target cell-type-specific effects remain to be characterized.

The essential role of NRG1 in the initiation of trabeculation is well documented, but its role in the cellular and molecular basis of trabecular growth, maturation, and resolution remains uncertain. In particular, understanding is limited about how morphological transitions occur and progress to yield a thick ventricular wall. Trabeculation mutations in mice invariably lead to fetal demise [41], precluding direct analysis of the mechanism(s) of trabecular growth and maturation.

Here, we used conditional and temporally regulated cardiac loss- and gain- of function mutants and transcriptomic profiling to show that NRG1 regulates early cardiomyocyte division by sustaining a transcriptional program that regulates cell polarity and cytoskeletal dynamics. NRG1 subsequently promotes trabecular expansion and initial ventricular wall thickening via dynamic changes in cardiomyocyte shape and movement, and fosters timely progression through the G1/S and G2/M phases of the cell cycle. We identify significant overlap between NRG1-dependent genes and conserved signatures of genes regulated by the ERBB2 receptor and the core MUVB-complex component LIN9, both of which act upstream or in conjunction with yes-associated protein-1 (YAP1). These findings suggest a complex interaction between NRG1-ERBB2/4-ERK and HIPPO-YAP1-LIN9 signaling that could be leveraged for future cardiac regeneration therapies.

METHODS

Full *Methods* are provided in the *Online Data Supplement*. Animal studies were approved by the CNIC Animal Experimentation Ethics Committee and by the Community of Madrid (Ref. PROEX 155.7/20). All animal procedures conformed to EU Directive 2010/63EU and Recommendation 2007/526/EC regarding the protection of animals used for experimental and other scientific purposes, enacted in Spanish law under Real Decreto 1201/2005.

RESULTS

NRG1-ERBB2/4-pERK signaling is required for trabeculae formation and expansion

To study the role of NRG1-ERBB2/4 signaling in cardiac development, we used a conditional *Nrg1*^{flox} mouse line [42] (see *Methods*). We crossed *Nrg1*^{flox} mice with the *Tie2*^{Cre} driver line [43] to conditionally inactivate *Nrg1* signaling in endothelial and endocardial cells from E7.5 onwards. At E8.5, there were no overt differences between control and *Nrg1*^{flox};*Tie2*^{Cre} embryos, both featuring a bilayered myocardial epithelium (Figure S1A,C). At E9.5, control hearts already showed nascent trabeculae and a double-layered compact wall (Figure 1A; Figure S1B). In contrast, *Nrg1*^{flox};*Tie2*^{Cre} mutants contained only a few trabecular projections, and the ventricular wall appeared somewhat thicker (Figure 1B,C; Figure S1D). By E10.5, the trabecular network in control ventricles had become more complex, whereas *Nrg1*^{flox};*Tie2*^{Cre} mutants had only a few thick, rudimentary trabeculae and a noticeably thicker compact myocardium, especially in the left ventricle (Figure 1A,B,F; Figure S1E,F). The profound differences in compact wall thickness and trabecular network size and complexity were also revealed by 3D-reconstructions (Figure 1D,E; Figure S1G,H; Movies S1 and S2). This defective trabecular phenotype was broadly reproduced in *Nrg1*^{flox} mice crossed with the cardiac cell-fate driver line *Mesp1*^{Cre} (Figure S2A-D). *Nrg1*^{flox};*Tie2*^{Cre} mutants died by E11.5 (Suppl. Table S1). E9.5 mutant hearts showed severely attenuated endocardial NRG1 expression (Figure 1G,H). This was reflected in reduced NRG1 signaling activity in the trabecular myocardium at E9.5, indexed by weak myocardial expression of phosphorylated ERBB2 (pERBB2) (Figure 1I,J) and of the phosphorylated intracellular effector ERK (pERK) (Figure 1K,L,M).

We further assessed pERK expression at key cardiac developmental stages as a readout of NRG1-pERBB2 activity [27, 34, 44, 45] (Figure S2E-I). At E9.5, intense but patchy pERK signals were detected in the myocardium, especially at the tips of trabeculae, but not in endocardium (Figure S2E). At E11.5, pERK expression was maintained along the trabeculae, especially at the tips (Figure S2F). At E12.5, strong pERK expression was found at the base of trabeculae (Figure S2G), suggesting a role in the formation of endocardially-derived coronary vessels. At E13.5, weak pERK expression was detected in a few myocardial cells, and stronger expression in the nascent coronaries (Figure S2H). At E16.5, pERK expression was almost exclusively limited to the coronary endothelium (Figure S2I).

The pERK temporal expression data are thus consistent with a function of NRG1 in trabecular myocardium between E9.5 and E12.5, and in coronary endothelium from E13.5 onwards.

NRG1 is required for cardiac development patterning and proliferation

To understand the basis of defective trabeculation in *Nrg1*^{flox};*Tie2*^{Cre} mutants, we examined the extracellular matrix (ECM) between endocardium and myocardium (the cardiac jelly), which is required for directional migration and the formation of cardiac trabeculae [28, 46, 47]. In control and *Nrg1*^{flox};*Tie2*^{Cre} hearts at E8.5, Alcian blue staining revealed the glycosaminoglycan constituent of the cardiac jelly (Figure S3A,C). However, at E9.5 and more obviously at E10.5, Alcian blue-staining was severely diminished in *Nrg1*^{flox};*Tie2*^{Cre} hearts compared with controls (Figure S3B,D,E,F), consistent with the manifestation of the trabeculation defect.

We next conducted an RNA sequencing (RNA-seq) analysis of E9.5 control and *Nrg1*^{flox};*Tie2*^{Cre} hearts. We found 1,166 differentially expressed genes (DEGs; 651 upregulated and 515 downregulated; $P<0.05$; Table S2, sheets 1 and 2). *Nrg1*^{flox};*Tie2*^{Cre} hearts showed severely depleted expression of *Nrg1* and several key cardiac developmental genes, including the trabecular marker genes *Bmp10, Hand1, Irx3,* and *Sema3a* (Figure 1N; Figure S3G). Also decreased in *Nrg1*^{flox};*Tie2*^{Cre} mutants was the expression of *Has2*, which participates in the synthesis of the cardiac jelly [46] (Figure 1N; Figure S3G). Consistent with these results, *Nrg1*^{flox};*Tie2*^{Cre} mutants showed altered expression of genes responsible for ECM turnover, either positively (*Adamts15*) or negatively (*Adamts12*) (Figure S3G). In situ hybridization (ISH) showed that *Has2* was restricted to rudimentary trabeculae in *Nrg1*^{flox};*Tie2*^{Cre} mutants (Figure S3H,I), as was the expression of *Bmp10*, *Hand1, Irx3,* and *Sema3a* (Figure 1P,Q; Figure S3J-M). In further agreement, *Nrg1*^{flox};*Tie2*^{Cre} mutants had markedly depleted expression of integrin alpha 6 (ITGα6) (Figure S3G,N-P), a trabeculae-restricted integrin [48]. In contrast, *N-myc* expression was increased in *Nrg1*^{flox};*Tie2*^{Cre} mutants (Figure 1N), and ISH revealed increased *Hey2* expression in the thicker compact myocardium of *Nrg1*^{flox};*Tie2*^{Cre} mutants, whereas the trabecular markers *Bmp10* and *Hand1* were restricted to a few cells in the primitive trabeculae (Figure 1P,Q). These results indicate that abrogation of NRG1-ERBB2/4 signaling disrupts trabeculae formation and chamber myocardium patterning.

To define the affected molecular mechanisms, we performed a GSEA of "HALLMARK" gene sets [49]. Most pathways were enriched (FDR q-val <0.05), including cellular stress pathways such as HYPOXIA and REACTIVE_OXYGEN_SPECIES_PATHWAY, ESTROGEN_RESPONSE_EARLY, MYC_TARGETS_V2, MTORC1_SIGNALING, and COAGULATION (Figure 1O; Table S2, sheet 3). These stress-response pathways are closely associated with activation of the P53_PATHWAY and E2F_TARGETS (Figure 1O; Figure S4A,B; Table S2, sheet 3). The P53 protein responds to stresses that disrupt the fidelity of DNA replication and cell division and initiates a program of cell cycle arrest, cellular senescence, or apoptosis [50]. Hence,

the genes contributing most to the enrichment score (the leading-edge genes) of the P53_PATHWAY were associated with upregulation of genes involved in the regulation of the cell cycle, DNA damage response, apoptosis, and other processes typical of the p53 response (Figure S4A). Genes associated with E2F_TARGETS were involved in the cell cycle, chromatin homeostasis, DNA repair, DNA replication, mitosis, and other processes, including cytoskeletal regulation (Figure S4B).

To determine whether proliferation was affected in *Nrg1*^{flox};*Tie2*^{Cre} hearts, we measured the incorporation of bromodeoxyuridine (BrdU, an S-phase marker) from E8.5 and E10.5 (Figure 1R,S; Figure S5A-E). At E8.5, the proliferation rate in mutant hearts was similar to that of control hearts (Figure S5A,B). At E9.5, a statistically significant 10% relative reduction in proliferation was detected in the compact myocardium of *Nrg1*^{flox};*Tie2*^{Cre} hearts (50% vs. 40%; Figure S5C-E). At E10.5, this difference persisted in compact myocardium (Figure 1R,S), whereas proliferation in the endocardium and trabecular myocardium was unchanged (Figure 1R,S). Trabeculation in zebrafish has been linked to pathways involving cell-shape changes and motility [1, 5, 51], and altered pathways in this category in *Nrg1*^{flox};*Tie2*^{Cre} hearts included KRAS_SIGNALING_UP, APICAL_SURFACE, ANGIOGENESIS, and EMT (EPITHELIAL_MESENCHYMAL_TRANSITION) (Figure 1O; Figure S4C,D; Table S2, sheet 3). Processes involving genes that regulate the cytoskeleton and ECM composition and metabolism tended to be depleted in E9.5 *Nrg1*^{flox};*Tie2*^{Cre} hearts, although this change was only evoked (FDR qval<0.5). (Figure1O, Figure S4C,D). These findings suggest that cardiomyocytes that normally contribute to trabeculae formation remain in the compact layer of *Nrg1*^{flox};*Tie2*^{Cre} mutants, leading to abnormal ventricular thickening at E9.5-10.5, despite the attenuated proliferation. Overall, the data indicate that NRG1-ERB2/4 signaling is required for both the patterning and emergence of trabeculae and the proliferation of compact layer cardiomyocytes.

NRG1 signaling is required for apicobasal cardiomyocyte polarity and cytoskeletal organization during trabeculation

Cell polarity and cytoskeletal dynamics are highly interconnected developmental processes [52], and alterations affecting them are associated with loss of trabeculation in mice and zebrafish [1, 47, 53]. We examined the RNA-seq data for potential changes in genes associated with the gene ontology (GO) set "CELL POLARITY" (GO:0030010) (Figure 2A). This analysis revealed misexpression in *Nrg1*^{flox};*Tie2*^{Cre} hearts of key genes required for cytoskeletal actin remodeling (*Arf4, Dock2, Sh3bp1, Arf6*), cytoskeletal organization (*Rac1, Rac2*), polarity (*Amotl1, Pard3, Nek3, Dlg1, Sipa1l3, Stk11, Wnt11*), division orientation (*Sapcd2*), motility (*Kif26b, Actr2*), and Fgf-ERK signaling (*Spry2, Fgf10*) (Figure 2A).

The altered expression of actin remodeling genes in *Nrg1*^{flox};*Tie2*^{Cre} mutants suggested the possibility of disrupted cardiomyocyte actin cytoarchitecture. Phalloidin staining of filamentous-actin (F-actin) in E8.5 control embryos revealed a uniform circumferential distribution of actin filaments

attached to the plasma membrane (Figure 2B,C, Movies S3,S5). In contrast, in *Nrg1*^{flox};*Tie2*^{Cre} hearts F-actin was non-uniformly distributed and appeared to concentrate in focal points at cell-cell junctions (Figure 2B,C, Movies S4,S6), suggesting that NRG1 is required for proper arrangement of the actin cortical network. Consistent with this actin cytoskeletal defect, *Nrg1*^{flox};*Tie2*^{Cre} mutants showed aberrant differential expression of genes sets for the GO terms for "Cytoskeleton" (GO:0005856) and "Regulation of actin polymerization" (GO: 0008064)(Figure S6A,B).

Nrg1^{flox};*Tie2*^{Cre} hearts showed reduced transcription of the key cell polarity regulator *Pard3* (Figure 2A, Table S2, sheet 2). *Pard3* inactivation leads to impaired apicobasal (A-B) polarity in epithelial cells [54] and planar polarity defects in endothelial cells [55]. "En face" examination of IF staining in E8.5 control hearts revealed evenly distributed PARD3 protein at the apical/abluminal pole of ventricular cardiomyocytes (Figure 2D left). In contrast, in *Nrg1*^{flox};*Tie2*^{Cre} hearts, PARD3 expression was strongly depleted (Figure 2D right), potentially disrupting A-B polarity. PARD3 immunofluorescence (IF) in heart sections confirmed localization to the apical/abluminal pole of wild type ventricular cardiomyocytes at E8.5 (Figure 2E), a distribution that was maintained at E9.5 in the compact layer, whereas trabecular cardiomyocytes did not express PARD3 (Figure S7A-C'). This observation fits with the loss of A-B polarity in cardiomyocytes that incorporate into nascent trabeculae [1]. In contrast, PARD3 staining was severely reduced in E8.5 and E9.5 *Nrg1*^{flox};*Tie2*^{Cre} ventricles (Figure 2E; Figure S7B-D'), further supporting the idea that A-B polarity is lost in mutant cardiomyocytes. A second polarity complex, Crumbs (CRB2A), has been shown to be required for the establishment of cardiomyocyte apicobasal polarity in zebrafish [56]. We readily detected CRB2 at the apical pole of the compact layer in E8.5 control cardiomyocytes (Figure 2F), but this expression was strongly depleted in *Nrg1*^{flox};*Tie2*^{Cre} mutants (Figure 2G), consistent with loss of A-B polarity in *Nrg1*^{flox};*Tie2*^{Cre} cardiomyocytes. These data indicate that ventricular trabeculation is mediated by NRG1-ERBB2/4–mediated regulation of genes required for A-B polarity and cytoskeletal network organization and turnover.

NRG1 is required for oriented division during trabeculation

Dynamic interplay between A-B polarity and adhesion complexes dictates both the positioning of the mitotic spindle during mitosis and the orientation of cell division [57]. Oriented cell division (OCD) and spindle orientation during trabeculation have been linked to the function and cellular distribution of N-Cadherin [6, 7, 53]. IF revealed a baso-lateral N-Cadherin distribution in the compact myocardium of control hearts at E8.5 and E9.5 (Figure 3A,B). In contrast, N-Cadherin was depleted at basal contact points in *Nrg1*^{flox};*Tie2*^{Cre} compact myocardium, while expression was maintained laterally (Figure 3A,B). Consistent with the disruption of adhesion complexes in *Nrg1*^{flox};*Tie2*^{Cre} mutants, the RNA-seq data revealed differential regulation of "Cell adhesion" (GO: GO:0007155) and "Regulation of cell-matrix adhesion" (GO: 0001952) (Figure S6C,D). These data suggest that NRG1-ERBB2 signaling is

required for N-Cadherin distribution at cardiomyocyte junctions during trabeculation, and further support the requirement of ERBB2 signaling for cell-junction integrity during trabeculation [53].

During trabeculation, ventricular cardiomyocytes divide obliquely or perpendicular to the lumen to give rise to the nascent trabeculae, whereas those that divide in parallel contribute to the outer compact myocardium [6, 47] (Figure 3C). We performed IF staining against Survivin to visualize the mitotic cleavage furrow and division axis during telophase (Figure 3D-Q). In E8.5 control hearts, 46.2% of mitotic cardiomyocyte divisions were parallel to the ventricular lumen (Figure 3D,P), whereas 26.9% were oblique (between 20-70º with respect to the lumen; Figure 3F,P) and 26.9% perpendicular (between 70-90º; Figure 3H,P). In contrast, in somite-matched E8.5 *Nrg1*^{flox};*Tie2*^{Cre} mutants, parallel divisions were significantly more frequent (76.7%; Figure 3E,P) and strong reductions were observed in oblique divisions (16.7%; Figure 3G,P) and perpendicular divisions (6.7%; Figure 3I,P). In E9.5 control embryos, parallel divisions remained predominant (61.4%) compared with perpendicular divisions (14%) or oblique divisions (24.6%; Figure 3J,L,N,Q). In E9.5 *Nrg1*^{flox};*Tie2-CRE* mutants, up to 83.6% of divisions were parallel and 14.5% were oblique (Figure 3K,M,Q), with perpendicular divisions significantly reduced to 1.8% (Figure 3O,Q). Cardiomyocyte OCD is thus disrupted in E8.5-E9.5 *Nrg1*^{flox};*Tie2*^{Cre} hearts, with parallel cardiomyocyte divisions favored at the expense of perpendicular divisions. We speculate that biased parallel division in *Nrg1*^{flox};*Tie2*^{Cre} mutants could offset the observed reduction of proliferation at E9.5 and lead to increased compact myocardium thickness.

NRG1 is required for formation of the inner ventricular wall formation but not the coronary vessels

Nrg1^{flox};*Tie2*^{Cre} embryos did not survive beyond E11.5 (Table S1, sheet 1), precluding analysis of late trabecular morphogenesis. To bypass this lethality, we bred *Nrg1*^{flox} and *Cdh5*^{CreERT2} mice [58] to obtain mice with tamoxifen-inducible endothelium-specific *Nrg1* deletion. Trabecular and compact wall growth was drastically hindered in E13.5 *Nrg1*^{flox};*Cdh5*^{CreERT2} mice after consecutive tamoxifen administration at E10.5 and E11.5 (Figure S8A). At E16.5, this phenotype manifested as thinner rudimentary trabeculae and a significantly reduced ventricular wall thickness (Figure 4A-C,E,F; Figure S8B-D). ISH analysis of the compact myocardium marker *Hey2* and the trabecular markers *Gja5* and *Bmp10* revealed loss of the molecular patterning of trabeculae in *Nrg1*^{flox};*Cdh5*^{CreERT2} mutants (Figure 4D; Figure S9A-D). Close inspection of the ventricular wall in *Nrg1*^{flox};*Cdh5*^{CreERT2} mutants further revealed the absence of the intermediate compact myocardium layer present in control ventricles (Figure 4E, ii). Later tamoxifen induction, at E12.5 and E13.5, did not result in any obvious structural abnormalities at E18.5 (Figure S9E,F). These data suggest that NRG1 is required from E9.5 to E13.5, both for trabecular growth and for the formation of an inner compact ventricular wall.

To determine the molecular basis of this phenotype, we performed an RNA-seq analysis on E15.5 control and *Nrg1*^{flox};*Cdh5*^{CreERT2} hearts (Figure 4G; Table S3, sheet 1). Differential expression analysis identified 40 upregulated and 30 downregulated genes (B-H p-value<0.05) (Table S3, sheet 2). Many expression differences were associated with pro-angiogenic and migratory processes (*Cxcr4, Vegfb*, *Aplnr1*, *Edn1, Ednrb*, and *Angpt1* [59-63]; Figure 4G) and the development of the ventricular conduction system (VCS; *Sema2a*, *Efna1, Nkx2-5, Etv1,* and *Ache* [64-68]; Figure 4G). Given that the endocardium gives rise to the ventricular inner wall vessels [12, 14] and that trabeculae differentiate into the cardiac Purkinje Fiber network [10], these data raise the possibility that loss of endothelial NRG1 expression from E11.5 onwards impairs the development both of the coronary arteries and of the VCS.

To assess the status of coronary vessel development in *Nrg1*^{flox};*Cdh5*^{CreERT2} mutants, we visualized the coronary network by whole-mount IF for IB4. In mice, the coronary arteries are located deep within the myocardial wall, whereas the veins are located superficially, beneath the epicardial layer [69]. This analysis revealed that the organization and complexity of the coronary arterial tree was not obviously affected in E16.5 *Nrg1*^{flox};*Cdh5*^{CreERT2} mutant hearts (Figure S10A,B,D). Likewise, IF analysis of the venous endothelial marker endomucin (Edmcn) also revealed no appreciable disturbance of venous tree organization in *Nrg1*^{flox};*Cdh5*^{CreERT2} hearts (Figure S10A,B,E). Similar results were obtained in the *Pdgfb*^{iCreERT2} vascular endothelium-specific CRE driver line ([70]; Figure S10A,C,D,E). We used SM22 and NOTCH3 immunostainings to determine the extent of coronary vessel smooth muscle cell differentiation and pericyte coverage, respectively [69]. Consistent with the absence of coronary defects, these parameters were comparable between *Nrg1*^{flox};*Cdh5*^{CreERT2} and control hearts (Figure S10F,G).

These data thus indicate that lack of an inner compact wall in *Nrg1*^{flox};*Cdh5*^{CreERT2} hearts does not appreciably impact development of the coronary tree. A reasonable interpretation is that the below-normal endocardial contribution to coronary vasculogenesis in these mutants is balanced by compensatory mechanisms involving alternative sources of endothelial cells [71].

NRG1 regulates motility and cell-cycle progression during ventricular wall growth

To identify mechanisms underlying the *Nrg1*^{flox};*Cdh5*^{CreERT2} phenotype, we performed GSEA. Among the "HALLMARK" gene sets, the most depleted pathway was "EMT" (-log(FDR) p-value < 0.05; Figure 4H; Table S3, sheet 3). The subset of leading-edge depleted genes was associated with cell cytoskeleton, ECM composition, modifiers of the ECM, and transmembrane and secreted proteins including adhesion molecules (Figure S11A). Also depleted were other depleted gene sets evoking cell shape and polarity, like "APICAL_SURFACE" and "APICAL_JUNCTION", and relevant pro-migratory signaling pathways, like "WNT_BETA_CATENIN_SIGNALING" and "HEDGEHOG_SIGNALING" (Figure 4H). Furthermore, the depletion of "CHOLESTEROL_HOMEOSTASIS" is consistent with the essential role of NRG1-ERBB4 signaling

in cholesterol metabolism [72]. In contrast, over-represented pathways, such as "G2/M_CHECKPOINT" and "E2F_TARGETS", are suggestive of cell-cycle alterations (Figure 4H). The subset of leading-edge upregulated genes included genes linked to the cell cycle, chromatin, DNA damage response, DNA repair, DNA replication, and mitosis (Figure S11B). Other prominent categories included nuclear transport and transcription regulation pathways and, importantly, the cytoskeleton (Figure S11B,C), emphasizing the nucleus-cytoskeleton connection. To support this finding, we examined E16.5 *Nrg1*^{flox};*Cdh5*^{CreERT2} mutants for possible alterations to the G2/M and G1/S cell-cycle phases by respectively counting myocardial cells positive for the early mitosis marker phospho-histone H3 (pH3) and measuring BrdU incorporation. Compared with stage-matched control hearts, E16.5 *Nrg1*^{flox};*Cdh5*^{CreERT2} hearts contained a markedly higher proportion of pH3+ cells, especially in trabeculae (Figure 4I,J), but there was no alteration in the proportion of BrdU+ cells in compact or trabecular myocardium, either at E13.5 (Figure S12A-D,I) or at E16.5 (Figure S12E-I). These data suggest that cell-cycle progression through the G2/M phase is delayed or prolonged in *Nrg1* mutants, while the G1/S phase is unaffected.

Overall, the analysis of the *Nrg1*^{flox};*Cdh5*^{CreERT2} transcriptome suggests that NRG1 regulates trabecular growth and chamber wall formation by coordinating cell migration and G2/M phase progression.

Ectopic NRG1 expression trabeculates myocardium and arrests cardiac development

To gain further insight into the role of NRG1 in chamber development, we created a conditional NRG1 gain-of-function model. For this, we generated a transgenic line bearing a *Rosa26-floxNeoSTOPflox-NRG1-EGFP* expression cassette (Figure S13A,B; see *METHODS*). Nkx2-5^{Cre}-mediated removal of the NeoSTOP sequence resulted in the expression of both the GFP reporter (Figure S13C,D) and NRG1 (Figure S13E,F). Examination of E16.5 embryos showed that *R26Nrg1*^{GOF};*Nkx2-5*^{Cre} transgenic hearts were developmentally arrested, with an appearance similar to that of E12.5 wild-type hearts (Figure S14A). This developmental arrest was further evidenced by the presence of ventricular septal defects (muscular and peri-membranous; Figure 5A,B), a double-outlet right ventricle, and an overriding aorta (Figure S14A). *R26Nrg1*^{GOF};*Nkx2-5*^{Cre} transgenic hearts also displayed superficial outgrowths resembling fistulae (Figure S14Ai,ii), which were possibly manifestations of direct communication between the endocardium and epicardium caused by considerable thinning of the compact myocardium (Figure 5A,B,E). Instead of a single cell layer, the transgenic epicardium consisted of 3–4 cell layers (Figure S14B), and the sub-epicardial layer was extensively infiltrated by endothelial cells but devoid of coherent large vessel conduits (Figure 5A,B; Figure S14B). Cardiomyocyte morphology (roundness) in the outer compact myocardium of *R26Nrg1*^{GOF};*Nkx2-5*^{Cre} transgenic hearts resembled more the trabecular myocardium of controls than the corresponding compact myocardium (Figure 5C,D,F). Moreover, expression of ITGα6 was expanded in E10.5

R26Nrg1^{GOF}*;Nkx2-5*^{Cre} hearts from the trabeculae to the compact layer (Figure S14C,D). Thus, NRG1 overexpression causes the compact myocardium to become trabeculae-like.

To determine the molecular underpinnings of this striking phenotype, we performed RNA-seq on E15.5 hearts. Differential expression analysis identified > 4,500 DEGs in *R26Nrg1*^{GOF}*;Nkx2-5*^{Cre} hearts (FDR q-value<0.05; Table S4). GSEA pathway analysis of "HALLMARK" gene sets revealed enrichment for pro-migratory processes suggested by "EMT", "APICAL_JUNCTION", and "KRAS_SIGNALING_UP" (Figure 5G). Enrichment for "IL6_JAK_STAT3_SIGNALING", "HYPOXIA", "IL2_STAT5_SIGNALING", and "UNFOLDED PROTEIN RESPONSE" reflected activation of cellular stress pathways, with "TNFA_SIGNALING_VIA_NFKB" and "APOPTOSIS" as possible outcomes. Moreover, "TGF_BETA_SIGNALING" and interrelated pathways like "INFLAMMATORY_RESPONSE" "COAGULATION", "COMPLEMENT", "ALLOGRAFT_REJECTION", and "INTERFERON_GAMMA_RESPONSE" are all hallmarks of cardiovascular disease (Figure 5G).

Conversely, several depleted pathways indicated impaired metabolic maturation, such as "OXIDATIVE_PHOSPHORYLATION", "FATTY_ACID_METABOLISM", "ADIPOGENESIS", "PROTEIN_SECRETION", "MYOGENESIS", and "CHOLESTEROL_HOMEOSTASIS" (Figure 5G), as well as "MYC_TARGET_V1" and "MYC_TARGET_V2", which link metabolism to the cell cycle (Figure 5G). To support these findings, we examined the intermediate filament protein NESTIN, a marker of cardiac immaturity [73]. In E16.5 control hearts, Nestin expression was weak in the trabecular myocardium but strong in developing epicardium (Figure S14E). In contrast, in *R26Nrg1*^{GOF}*;Nkx2-5*^{Cre} transgenic hearts, Nestin expression was substantial in trabecular myocardium and in compact myocardium devoid of α-smooth-muscle actin (SMA) staining (Figure S14F). This suggests that the relative proportion of constituent cell types is altered in the ventricular chamber walls of *R26Nrg1*^{GOF}*;Nkx2-5*^{Cre} embryos, suggesting a maturation defect.

The expression of the subset of His-Purkinje-specific genes [74] was broadly upregulated in *R26Nrg1*^{GOF}*;Nkx2-5*^{Cre} ventricles (Figure 5H). ISH analysis revealed expansion of *Gja5* transcription towards the compact myocardium (Figure 5I), consistent with a role of NRG1 as a driver of VCS specification and differentiation [75].

The depletion of cell-cycle–related gene sets, including "E2F_TARGETS" and "G2M_CHECKPOINT" (Figure 5G), also suggested a proliferation defect associated with the fetal developmental arrest of *R26Nrg1*^{GOF}*;Nkx2-5*^{Cre} embryos. The proportion of pH3+ cells was similar in E16.5 control and *R26Nrg1*^{GOF}*;Nkx2-5*^{Cre} transgenic hearts (Figure S14G-I), indicating that the G2/M phase of the cell cycle was unaffected. In contrast, the proportion of BrdU+ cells was lower in the compact and trabecular myocardium of *R26Nrg1*^{GOF}*;Nkx2-5*^{Cre} hearts (Figure 5J,K), suggesting either a decreased proliferation rate, or delayed G1/S progression. A reasonable interpretation is that the

proliferation rate across the ventricular wall is homogeneously reduced in *R26Nrg1*^{GOF}*;Nkx2-5*^{Cre} transgenic hearts, consistent with the suggested "trabeculation" of compact layer cardiomyocytes.

Thus, NRG1 overexpression slows the rate of cardiomyocyte proliferation and arrests fetal cardiac maturation.

NRG1 regulates ventricular patterning mediated by cytoskeletal dynamics

Analysis of chamber trabecular and compact myocardium markers revealed profoundly altered myocardial wall patterning in both the *Nrg1*^{flox}*;Cdh5*^{CreERT2} mutant and *R26Nrg1*^{GOF}*;Nkx2-5*^{Cre} transgenic hearts (Figure 6A-C). At E16.5, SMA is normally confined to the immature and proliferative compact myocardium ([76]; Figure 6D). However, SMA expression was extended along the length of trabeculae in E16.5 *Nrg1*^{flox}*;Cdh5*^{CreERT2} hearts (Figure 6E), consistent with the maintenance of compact myocardium identity and defective trabecular maturation. In contrast, SMA expression was markedly reduced in the compact myocardium of *R26Nrg1*^{GOF}*;Nkx2-5*^{Cre} transgenic hearts, (Figure 6F), in line with a loss of compact myocardium identity. In agreement with these findings, ISH showed that *Hey2* expression abnormally extended into the trabeculae of *Nrg1*^{flox}*;Cdh5*^{CreERT2} hearts, contrasting its normal restriction to the compact myocardium (Figure 6G,H), and was almost completely absent from *R26Nrg1*^{GOF}*;Nkx2-5*^{Cre} ventricles (Figure 6G,I), reflecting loss of compact myocardium identity. Conversely, *Bmp10* expression was attenuated in the trabeculae of *Nrg1*^{flox}*;Cdh5*^{CreERT2} mutants (Figure 6J,K) and extended into the compact layer in *R26Nrg1*^{GOF}*;Nkx2-5*^{Cre} transgenic embryos (Figure 6J,L), reflecting acquisition of trabecular identity. Thus, NRG1 loss of function causes trabecular myocardium to become compact-like, whereas NRG1 gain-of-function causes compact myocardium to become trabecular-like.

Sarcomeres consist of bundles of polymerized actin crosslinked by α-actinin at the Z-line and arranged in a stacked striated pattern throughout muscle tissue. In cardiomyocytes, sarcomeres are oriented transversely, allowing contraction and shortening of muscle cells along their longitudinal axis. We were thus able to infer muscle-cell orientation by using IF against α-actinin to visualize sarcomeres. Analysis of sarcomeres in the trabecular myocardium of control, loss-of-function (LOF), and gain-of-function (GOF) hearts showed similar random fiber orientation (Figure 6Mi, 6Ni, 6Oi). The compact myocardium of control hearts showed two layers of fibers according to their orientation, the inner compact myocardium (Figure 6Mii) and the outer compact myocardium (Figure 6Miii). *Nrg1*^{flox}*;Cdh5*^{CreERT2} hearts lacked the inner compact myocardial layer but retained a normal outer compact myocardium (Figure 6Nii, iii). In contrast, the compact myocardium of *R26Nrg1*^{GOF}*;Nkx2-5*^{Cre} ventricles showed random fiber orientation, similar to trabecular myocardium (Figure 6Oi-iii). Upon closer inspection, *Nrg1*^{flox}*;Cdh5*^{CreERT2} compact-myocardium sarcomeres appeared slightly more diffuse than their control counterparts and contained ring-like structures (Figure 6P,Qii,iii), suggesting disruption of Z-line alignment. The striated sarcomere structure revealed by α-actinin staining was also

broadly evident from F-actin staining, including the presence of ring-like structures in *Nrg1*^{flox}*;Cdh5*^{CreERT2} hearts (Figure 6Qii,iii), suggesting mis-arrangment of F-actin branching. Moreover, similar ring-like structures were detected in the compact-myocardium sarcomeres of *R26Nrg1*^{GOF}*;Nkx2-5*^{Cre} transgenic hearts (Figure 6Rii,iii). Overall, these data indicate that above-normal or below-normal NRG1 expression disrupts sarcomere Z-line positioning, consistent with NRG1 being required for sarcomere structural integrity and maturation.

NRG1 modulates pERK-dependent YAP1 S274 phosphorylation during trabeculation

Having identified myocardial pERK as a read-out of NRG1 signaling during trabeculation (see Figures S2E-I; Figure 1K-M), we monitored pERK expression in *R26Nrg1*^{GOF}*;Nkx2-5*^{Cre} transgenic hearts. In control hearts, pERK was expressed in trabeculae and cardiomyocytes close to the ventricular lumen at E9.5 (Figure 7A), and additionally in some epicardial cells at E11.5 (Figure 7C). In contrast, E9.5-E11.5 *R26Nrg1*^{GOF}*;Nkx2-5*^{Cre} transgenic hearts showed ectopic pERK expression in the compact myocardium and sub-epicardial layers (Figure 7B,D). From E13.5 onwards, pERK was no longer detected in the myocardium of control hearts (Figure S2H,I), but was expressed in coronary endothelial cells (Figure S15A), similarly to the observation in *Nrg1*^{flox}*;Cadh5*^{CreERT2} hearts (Figure S15B). At E16.5, pERK was no longer expressed ectopically in *R26Nrg1*^{GOF}*;Nkx2-5*^{Cre} myocardium (Figure S15C). In addition, E18.5 *Nrg1*^{flox}*;Cdh5*^{CreERT2} mice developed a normal heart after tamoxifen administration at E12.5 and E13.5 (Figure S9E,F), suggesting that NRG1–pERK signaling is required for chamber development at an earlier stage.

To support these findings, we examined the expression of pERBB2 and pERBB4 during compaction. In E16.5 control hearts, pERBB2 and pERBB4 were both strongly expressed in coronary endothelium, sparsely expressed in endocardium, and absent from myocardium (Figure S15D,G). pERBB2 was also readily detected in epicardium (Figure S15D). In *Nrg1*^{flox}*;Cadh5*^{CreERT2} hearts, the strong coronary endothelial expression and sparse endocardial expression were maintained (Figure S15E,H). In *R26Nrg1*^{GOF}*;Nkx2-5*^{Cre} hearts, strong pERBB2 and pERBB4 expression was detected in both endothelium and endocardium, and remained absent from myocardium (Figure S15F,I). Thus, during compaction, pERBB2 and pERBB4 are no longer expressed in myocardium, and cannot be induced by NRG1 in this tissue.

We noticed that the *R26Nrg1*^{GOF}*;Nkx2-5*^{Cre} gene signature closely mirrored gene signatures found in adult mouse hearts overexpressing the ERBB2 receptor (ERBB2^{OE}) [77] and in fetal hearts deficient for the activator MuvB core complex component Lin9 (Lin9^{KO}) [78] (Figure 7E,F). Notably, the EMT and oxidative phosphorylation gene signatures were respectively enriched and depleted in the transcriptomes of all three of these models (Figure 7E-G), whereas the opposite change occurred after NRG1 deletion (Figure 7G). ERBB2-mediated cardiac regenerative phenotypes are mediated, in part, by YAP1 [77], and there is significant overlap between the conserved YAP-regulated gene signature

and LIN9-dependent genes [79]. GSEA revealed that many of the differentially-regulated genes in ErbB2^{OE} and Lin9^{KO} hearts were also significantly altered in the NRG1 LOF and GOF transcriptomes (Figure 7H). Moreover, the E15.5 *R26Nrg1^{GOF};Nkx2-5^{Cre}* transcriptome also showed overlap with the YAP1 target gene signature [80] (Figure 7H). Part of this enriched gene signature corresponded to the EMT pathway (Figure 7G), suggesting that a significant portion of the NRG1 transcriptome involving cytoskeletal genes might also be YAP-dependent.

The activation/inactivation of YAP by canonical HIPPO-dependent and non-HIPPO dependent phosphorylations has been linked to mechano-transduction and mitosis during cardiac regeneration [77]. ERBB2 signaling via ERK elicits cytoskeletal changes with an altered mechanical state and downstream YAP S274 phosphorylation, resulting in pYAP activation and nuclear localization [77]. Given the enrichment of YAP-target genes in *R26Nrg1^{GOF};Nkx2-5^{Cre}* hearts, we examined the NRG1 LOF and GOF mutants for HIPPO (MOB1)-dependent YAP1 phosphorylation on S112 (S127 in human) and pERK and mitosis-associated YAP1 phosphorylation on S274 (S289 in human) [81, 82]. In control E9.5 hearts, pYAP S112 was strongly expressed in the cytoplasm of endocardial cells and weakly expressed in some cardiomyocytes (Figure S16A). In *Nrg1^{flox};Tie2^{Cre}* hearts, pYAP S112, while maintained in endocardium, was no longer expressed in cardiomyocytes (Figure S16B). Interestingly, pMOB1-Thr35 expression was also below normal (Figure 7K), suggesting that HIPPO-dependent YAP1 nuclear localization would be higher in E9.5 *Nrg1^{flox};Tie2^{Cre}* hearts. However, at E13.5, pYAP S112 was present exclusively in endocardial cells in both control and *Nrg1^{flox};Cadh5^{CreERT2}* hearts (Figure S16C,D), and the same restriction was observed at E16.5 in control and *R26Nrg1^{GOF};Nkx2-5^{Cre}* hearts (Figure S16E,F). pYAP S112 expression and HIPPO pathway activity are thus dependent on NRG1 at E9.5, but independent of NRG1 at E13.5 and E16.5.

At E9.5, pYAP S274 was localized in the nuclei of myocardial cells in control hearts (Figure 7I) but was mostly cytoplasmic in *Nrg1^{flox};Tie2^{Cre}* hearts (Figure 7J). In agreement with this, western blot analysis revealed below-control pYAP S274 expression in *Nrg1^{flox};Tie2^{Cre}* hearts (Figure 7K). Consistent with the dependence of pYAP S274 on ERK phosphorylation [77], pERK expression was also below control (Figure 1M). In contrast, at E16.5, pYAP S274 IF labeled only scattered cells in the myocardium of control, *Nrg1^{flox};Cdh5^{CreERT2}*, and *R26Nrg1^{GOF};Nkx2-5^{Cre}* hearts (Figure 7N-P). At this stage, western blot analysis also detected control-level expression of pMOB1-Thr35 in NRG1 LOF and GOF mutants (Figure 7L,M).

These data indicate that myocardial ERK phosphorylation, pYAP S274 cellular distribution, and HIPPO/MOB1 activity are dependent on NRG1 during trabeculation but not during compaction.

Discussion

The results presented here show that NRG1 regulates ventricular trabeculation by acting as a paracrine signal to generate a distribution of polarized morphologies and division dynamics across the ventricular wall. Our dissection of the mechanisms giving rise to trabecular and non-trabecular myocardium reveal that NRG1 transcriptionally regulates cell-cycle and EMT-like transcriptional programs required for cardiomyocyte A-B polarity, oriented cell division, and directional migration (Figure 8).

We interpret our findings in light of a body of work showing that the formation of trabeculae is a highly dynamic process involving transient disruption of the integrity of the primitive myocardial cell layer. Trabeculation in zebrafish is an EMT-like process that involves dynamic changes in the actin cytoskeleton network, resulting in actomyosin polarization, directional apical constriction, depolarization, and delamination without division [1, 3-5, 51, 83]. In mice, the realignment of the mitotic spindle and dividing axis of trabeculating cardiomyocytes involves transient disruption and re-positioning of A-B polarity and focal cell and matrix adhesion complexes [6, 7, 47]. Furthermore, interlinked posttranscriptional and transcriptional cascades converge to drive dynamic changes in the contractile actomyosin network, influence force transmission, and control spindle orientation and directional migration [52, 84, 85].

We infer from our transcriptomics data that NRG1 regulates a morphogenetic process involving changes in cell behavior and/or shape, and whose disruption leads to profound changes in cardiomyocyte architecture. Our early stage LOF experiments show that NRG1 regulates the transcription of genes required for cell shape and morphology, including key components of polarity complexes, with NRG1 LOF leading to the depletion of the apical junction and polarity proteins PARD3 and CRUMBS2, which have been linked to trabeculation [47, 56] (Figure 8). These changes were further associated with evidence of ventricular wall defects and altered redistribution of intercellular connections established by the cell junctional protein N-CADHERIN, which is required for structural integrity of the myocardium [6, 7, 53]. Finally, the disordered actin cytoarchitecture in NRG1 mutants resulted in failure to acquire the motile and invasive behaviors required for trabeculation.

Our later stage conditional LOF experiments suggest that trabecular growth and elongation phases are driven by EMT-like migration of cardiomyocytes derived from the growing outer compact layer towards the trabecular base (Figure 8), consistent with previous analyses identifying clones of cells spanning anatomical transmural locations during ventricular chamber formation [6, 8, 83, 86, 87]. These EMT-like processes involve disruption of cell–cell interactions at adherens junctions and disassembly of the polarity complexes that define the cardiomyocyte apical-lateral and basal-lateral domains, with rearrangement of actin filaments to bestow motile and invasive behaviors as an element of the core changes required for cellular motility [88]. However, these changes take place in the absence of the activation of specific transcription factors or the acquisition of mesenchymal markers and do

not involve the establishment of a front-to-back polarity as normally occurs during EMT, suggesting that this type of EMT is partial or incomplete [88].

We found that trabecular growth depends on the initial thickening of the myocardial wall by an intermediate layer consisting of mixed trabecular and compact zone cardiomyocytes. The outer compact myocardium initially consists of just 2-3 layers, but attains a thickness of about 15-20 cell layers by the end of trabeculation (Figure 8), likely through differential growth [89]. We surmise that the intermediary layer acts as the precursor layer for trabecular growth, based on evidence of transmural clones originating from the outer "feeder" layer [6]. Thus, through transcriptional regulation of cell polarity, cell-cell and cell-matrix adhesion, and cell migration, NRG1 regulates the myocardial spatial distribution of compact and trabecular myocardium by generating molecularly distinct myocardial layers and establishing the boundaries of trabecular identity (Figure 8).

Consistent with this notion, our GOF experiments show that, by promoting the development of the trabecular and intermediary layers, NRG1 restricts the growth of the self-expanding cardiomyocytes of the outer layer. As development progresses, proliferation of the outer compact layer is no longer dependent on NRG1 or other signals emanating from the endocardium. By virtue of their comparatively higher proliferation rate, compact layer cardiomyocytes eventually outnumber trabecular cardiomyocytes during the compaction phase of ventricular wall development [13]. Thus, the influence of NRG1 gradually becomes limited to the endocardium-proximal cardiomyocytes that give rise to the subendocardial ventricular myocardium and Purkinje fiber conduction system network [74] (Figure 8). Specification to trabecular versus compact myocardium may depend on the relative distance of cardiomyocytes from the source of NRG1.

Likewise, the patterning and growth of the compact myocardial layer(s), whose specification does not depend on NRG1 [90, 91], requires signals from the epicardium. Thus, NRG1 overexpression resulted in a profound change in compact ventricular wall composition, increasing the proportion of endothelial and epicardial cells while seemingly reducing that of cardiomyocytes. This suggests that, by the end of trabeculation (E12.5-E13.5), cardiomyocytes are no longer sensitive to NRG1, as evidenced by the suppression of the activation of the downstream effector pERK in the myocardium. This likely occurs through downregulation of the ERBB2/4 receptors, and would be consistent with a spatio-temporal range of action largely confined to the trabecular period of ventricular wall development.

Our studies further highlight the tight coordination between cell division and migration that evolved to ensure pattern and boundary formation during tissue growth and morphogenesis [92-96]. Consequently, we found that, in addition to the morphogenic EMT-like component, NRG1 regulates gene signatures for cell-cycle progression linked to mitosis, DNA replication and repair, and the cytoskeleton [97-99]. The early NRG1 LOF trabecular phenotype was associated with the activation of prominent cell stress pathways and p53, whose activation can lead to cell-cycle arrest at G1/S and

G2/M [100]. However, we interpret activation of this pathway as a consequence of the strong hypoxic response taking place in the absence of NRG1. Nevertheless, the NRG1 LOF transcriptomes were also associated with activation of E2F and MYC, which have roles in DNA replication and mitotic function [101, 102] and have a complex cross-regulatory relationship in cell-cycle progression [103]. In addition, there is a close association between cytoskeletal organization, cell adhesion, and the cell cycle [104], revealed by G2/M checkpoint controls regulated by actin dysfunction [105-109]. Our interpretation of the hypoplastic conditional LOF mutant phenotype is plausible if we take into account the existence of such a checkpoint control and the requirement of NRG1 for progression through the G2/M phase. Consistent with this idea, ERBB2 (HER2) and ERK1/2 have been identified as important regulators of the G2/M checkpoint response to γ-irradiation [110, 111].

A number of key observations can be gleaned from the available evidence: 1) NRG1 activates endogenous ERBB4 to induce YAP1 target genes in breast cancer cells [72]; 2) ERBB2 drives ERK-dependent and HIPPO-independent YAP1 activation and mitosis during cardiac regeneration [77]; 3) Interaction of YAP1 with the Myb-MuvB (MMB) complex promotes the expression of G2/M (mitotic) phase genes in fetal cardiomyocytes [78]; and 4) YAP1-mediated cardiac regeneration requires the transcription of cell-cycle, adherens-junction, and cytoskeletal genes [80, 112-114]. We suggest that YAP1 is a downstream effector of NRG1 during trabeculation (Figure 8). We found significant overlap between the gene signatures of $NRG1^{GOF}$ and that of ERBB2 and YAP overexpression and Lin9 inactivation, mainly involving EMT-like pathway genes. Our studies of pYAP S274 nuclear-cytoplasmic localization provide preliminary evidence that NRG1 is required for YAP1 nuclear localization during early trabeculation but not during compaction, consistent with a restricted NRG1-pERK window of function. Intriguingly, the YAP1 homolog WWTR1 promotes compact wall development by inhibiting trabeculation in zebrafish, whereas NRG1-ERBB2 signaling negatively regulates WWTR1 nuclear localization and activity [31]. These findings provide incentives for further studies into the role of NRG1-YAP1 in ventricular wall development.

Our studies provide evidence that noncompaction/hypertrabeculation is a defect of asymmetric ventricular wall growth. Because of the considerable overlap between trabeculation and ventricular wall maturation and compaction, it has been difficult to distinguish the excessive trabeculation phenotype from the failure to compact and to determine whether these phenotypes form part of a continuum or are separate entities. Experimental evidence from hiPSC models suggests that non-compaction might be attributable to defective cardiomyocyte proliferation [115], whereas data from mice show that the persistence of trabeculae postnatally may be the result either of excessive proliferation of trabecular cardiomyocytes [116, 117] or of reduced proliferation of the compact myocardium [13, 20, 118]. Our studies help to resolve this conundrum by suggesting that non-compaction/hypertrabeculation

is linked to a disruption of asymmetric growth and differentiation across the ventricular wall, resulting in defective trabecular patterning and differential cardiomyocyte proliferation.

In summary, NRG1 ensures oriented cell division and migration by driving cell polarity and adhesion programs. The prominent processes involved in the trabecular phase between E9.5 and E13.5 resembled EMT, evoking changes in cell morphology, cell movement, and a reorientation of the plane of cell division. Moreover, NRG1 coordinates cell dynamics and proliferation during ventricular wall development, essential for the specification of trabecular and non-trabecular cardiomyocytes. The extensive overlap between cell division and morphogenesis makes it difficult to discern the individual contributions of these processes to trabecular and compact myocardium growth. The possibility of multi-omic measurement at single-cell scale provides an incentive for future investigation.

Acknowledgments

We thank A. Galicia and L. Méndez for mouse husbandry, the Genomics Units for carrying out RNA-seq, and S. Bartlett for English editing.

Sources of Funding

This study was supported by grants PID2019-104776RB-I00 and PID2020-120326RB-I00, CB16/11/00399 (CIBER CV) from MCIN/AEI/ 10.13039/501100011033, a grant from the Fundación BBVA (Ref.: BIO14_298), a grant from Fundació La Marató de TV3 (Ref.: 20153431) and a grant from the Spanish Society for Cardiology (SECSCFG-INV-CFG 21/004) to J.L.d.l.P. J.G-B. was funded by Programa de Atracción de Talento from Comunidad de Madrid (Ref. 2016T1/BMD1540). The cost of this publication was supported in part with funds from the European Regional Development Fund. The CNIC is supported by the ISCIII, the MCIN and the Pro CNIC Foundation and is a Severo Ochoa Center of Excellence (grant CEX2020001041-S) financed by MCIN/AEI /10.13039/501100011033.

Disclosures None.

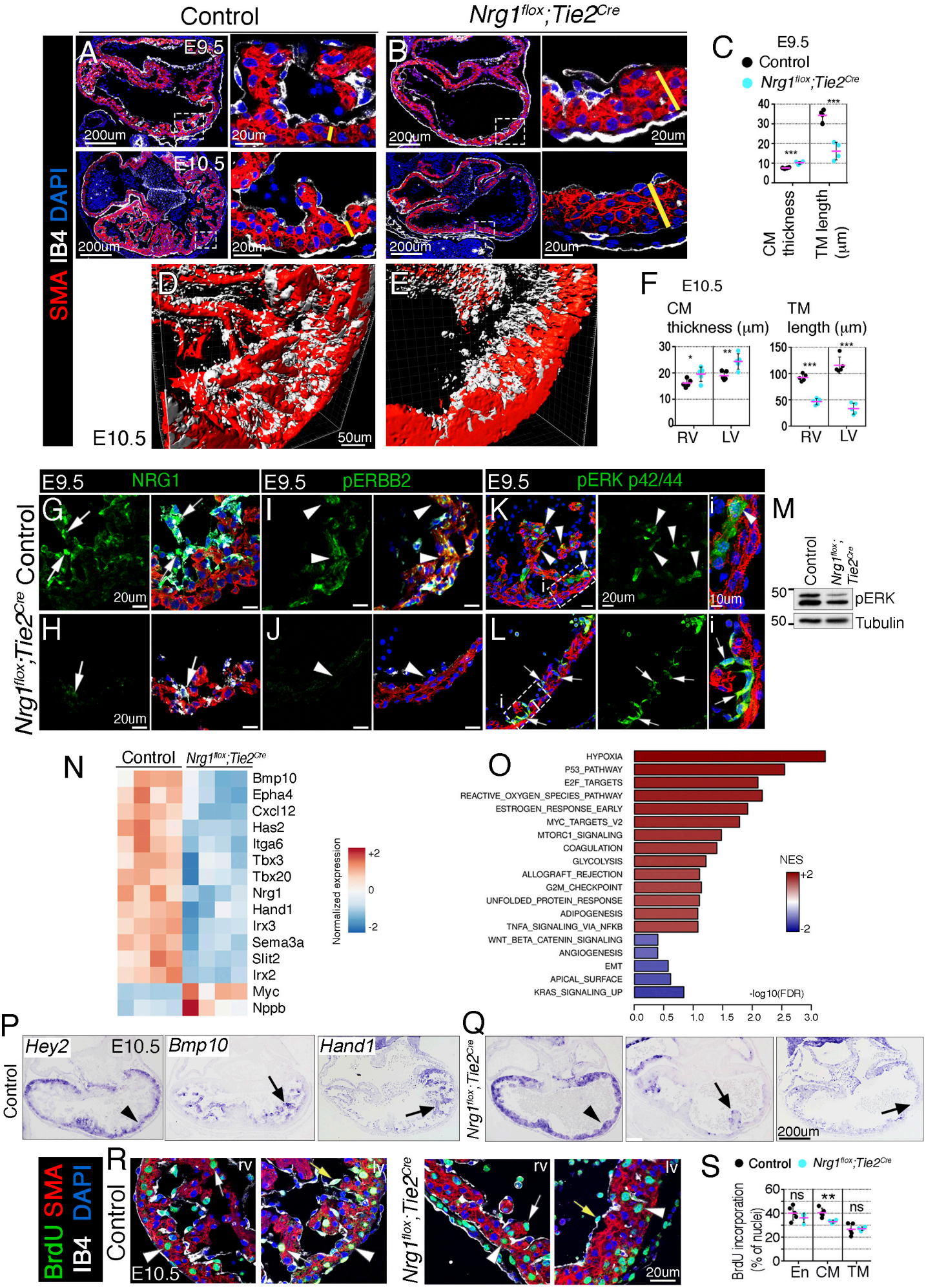

Figure 1_Grego-Bessa

Figure Legends

Figure 1. NRG1-ERBB2-pERK signaling is required for trabeculation initiation and expansion. **(A,B)** Immunofluorescence against smooth muscle actin (SMA, red) and isolectin B4 (IB4, white) in heart sections from E9.5 and E10.5 control **(A)** and *Nrg1*^{flox}*;Tie2*^{Cre} embryos **(B)**. Yellow lines mark the thickness of the compact myocardium (CM). Sections were counterstained with DAPI (blue). **(C)** Quantification of CM thickness and trabecular myocardium (TM) length in control and *Nrg1*^{flox}*;Tie2*^{Cre} left ventricles at E9.5. **(D, E)** 3D reconstruction of SMA-stained E10.5 control and *Nrg1*^{flox}*;Tie2*^{Cre} left ventricles. **(F)** Quantification of CM thickness and TM length in control and *Nrg1*^{flox}*;Tie2*^{Cre} ventricles at E10.5. **(G-L)** Immunofluorescence against Nrg1, pERBB2, and pERK (green) in E9.5 control embryos **(G, I, K)** and *Nrg1*^{flox}*;Tie2*^{Cre} embryos **(H, J, L)**. SMA, red; IB4, white; DAPI counterstain, blue. Arrows mark endocardium, arrowheads myocardium. **(M)** Representative western blot of pERK in E9.5 ventricles (pool of n = 3 per genotype). **(N)** Heatmap of representative differentially expressed genes (DEGs) in E9.5 control vs. *Nrg1*^{flox}*;Tie2*^{Cre} hearts. The color code represents normalized gene expression from -2 to $\pm$ 2. **(O)** Hallmark Gene Set Enrichment Analysis (GSEA) for E9.5 *Nrg1*^{flox}*;Tie2*^{Cre} vs. Control. The bar plot represents enrichment data for 19 Hallmark gene sets at a false discovery rate FDR qval < 0.1 and FDR qval < 0.5, for gene sets with positive or negative enrichment score, respectively. Of those gene sets, 8 had an FDR qval < 0.05. The scale bar represents normalized enrichment score (NES) from -2 to $\pm$2. Positive scores (red), indicating enrichment in *Nrg1*^{flox}*;Tie2*^{Cre} relative to the control condition, were found for 14 gene sets, and negative scores (blue), indicating depletion, were found for 5 gene sets. Relative expression values for the "leading edge" genes associated to gene sets P53_PATHWAY, E2F_TARGETS, KRAS_SIGNALING_UP and EMT are presented as heatmaps in figure S4. **(P,Q)** ISH of *Hey2*, *BMP10*, and *Hand1* in E9.5 control embryos **(P)** and *Nrg1*^{flox}*;Tie2*^{Cre} embryos **(Q)**. Arrows mark TM, arrowheads CM. **(R)** Immunodetection of BrdU in E10.5 control and *Nrg1*^{flox}*;Tie2*^{Cre} embryos. Arrows mark myocardium, arrowheads endocardium. **(S)** Quantification of BrdU incorporation in E10.5 control embryos (n=4) and *Nrg1*^{flox}*;Tie2*^{Cre} embryos (n=3). En, endocardium; RV, right ventricle; LV, left ventricle. * $P < 0.05$, ** $P < 0.01$, $P < 0.001$; ns, non-significant by Student t-test. Scale bars=200 μm (low magnification in A,B, and P,Q); 50μm (D,E); 20 μm (high magnification in A,B and G, I, K H, J, L, and R).

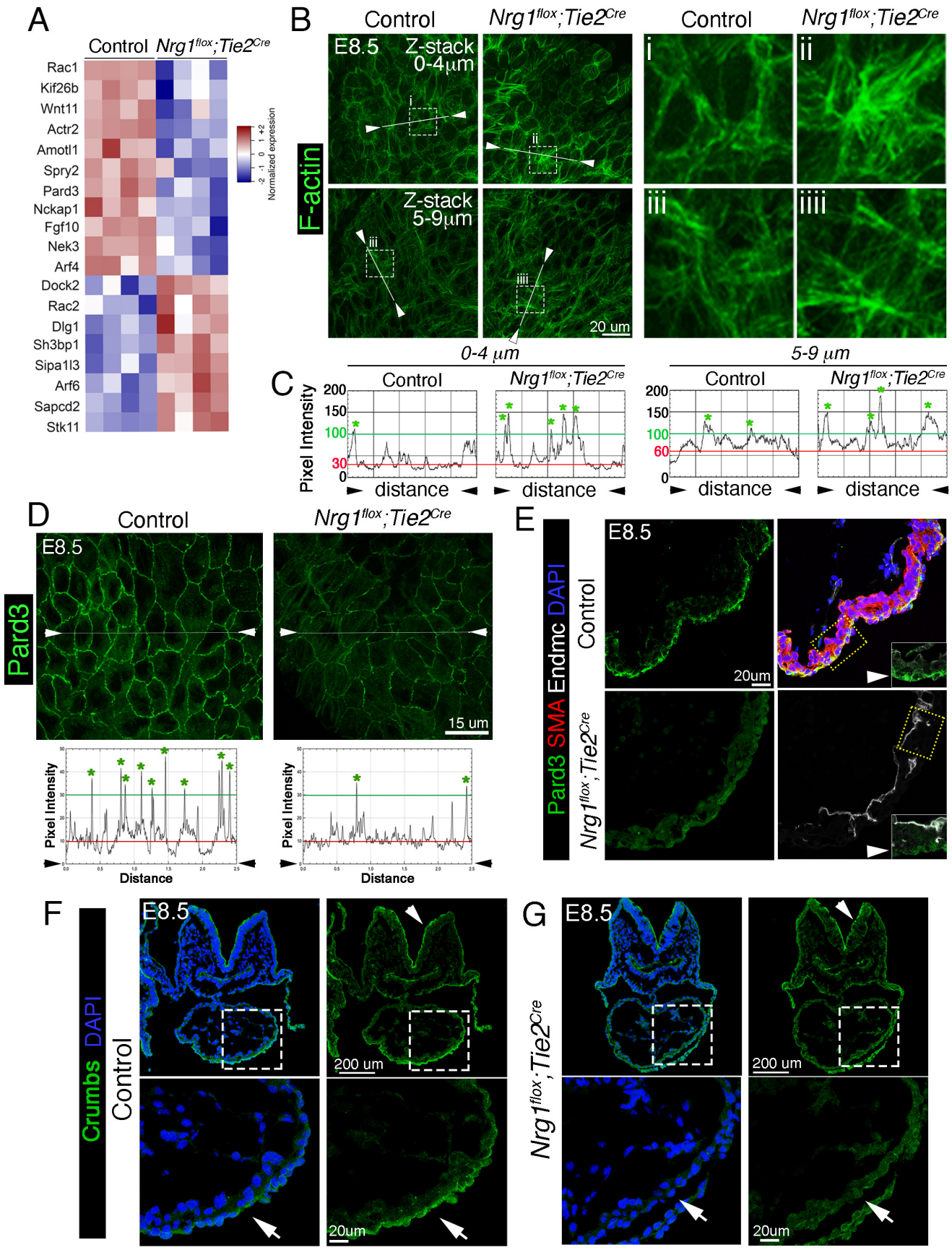

Figure 2_Grego-Bessa

Figure 2. NRG1 is required for apicobasal polarity and cytoskeletal organization during trabeculation. (A) Enrichment analyses performed with Panther on the set of genes detected as "Establishment or maintenance of cell polarity" (GO:0007163; pval = 0.0064). The heatmap represents relative expression values for differentially expressed genes annotated with this GO term. **(B)** Whole mount phalloidin staining Z-stack projections of apical regions (from 0 to 4 μm) and baso-lateral regions (5 to 9 μm) of outer compact myocardium in E8.5 control and *Nrg1*^{flox}*;Tie2*^{Cre} heart sections. **(C)** Quantification of pixel intensity along a 10-pixel-wide trace (white lines in B). Red lines indicate that background intensities in control and *Nrg1*^{flox}*;Tie2*^{Cre} heart sections are similar. Green asterisks indicate values above gray intensity=100 (green lines). **(D)** Whole mount immunofluoresence of Pard3 in E8.5 control and *Nrg1*^{flox}*;Tie2*^{Cre} heart sections. Charts below, quantification of pixel intensity along a 10-pixel-wide trace (white lines between arrowheads). Red lines indicate that background intensities in control and *Nrg1*^{flox}*;Tie2*^{Cre} heart sections are similar. Green asterisks indicate values above gray intensity=30 (green lines). **(E)** Immunofluoresence of Pard3 in transverse sections of E8.5 control and *Nrg1*^{flox}*;Tie2*^{Cre} embryos (green). Arrowheads mark the apical domain of the compact myocardium. SMA, smooth muscle actin; Endmc, endomucin (white). DAPI counterstaining is shown in blue. **(F-G)** Immunofluoresence against Crumbs in transverse sections of E8.5 control and *Nrg1*^{flox}*;Tie2*^{Cre} embryos (green). DAPI counterstaining is shown in blue. Arrowheads mark the apical domain of the neural tube and indicate similar signal intensities. Arrows mark the apical domain of the compact myocardium. Scale bars=20 μm (B, E, F and G); 15 μm (D).

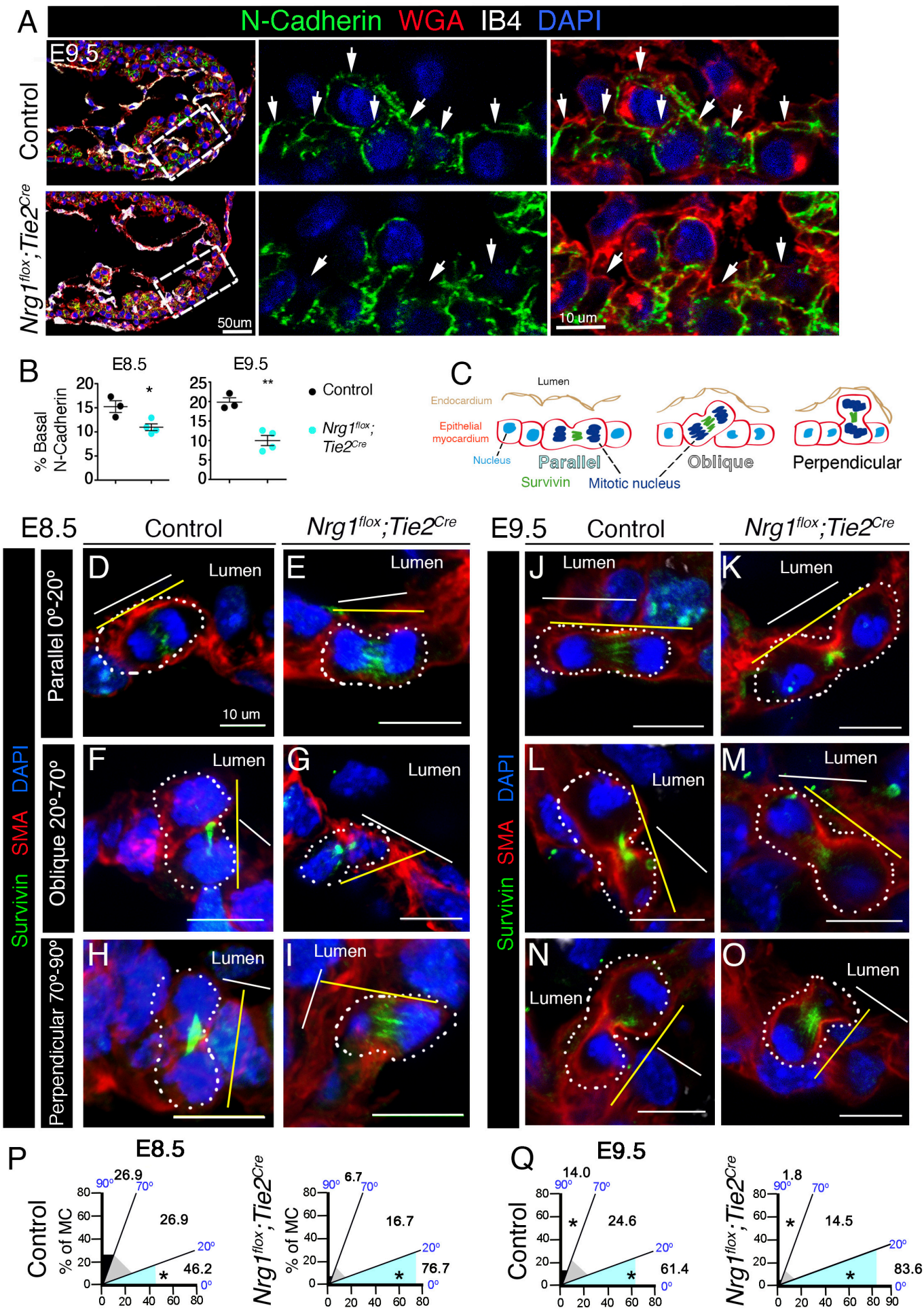

Figure 3_Grego-Bessa

Figure 3. NRG1 is required for oriented division during trabeculation. (A) Immunofluorescence against N-Cadherin and wheat germ agglutinin (WGA) on E9.5 control and *Nrg1*^{flox}*;Tie2*^{Cre} heart sections. Arrows mark the cardiomyocyte basal layer, facing the cardiac lumen. Scale bars=(A) 50 μm (low magnification) and 10 μm (high magnification)**. (B)** Quantification of basal layer N-Cadherin in control and *Nrg1*^{flox}*;Tie2*^{Cre} hearts at E8.5 and E9.5. **P* < 0.05; ** *P* < 0.001 by Student t-test. **(C)** Schematic of the analysis of mitotic-spindle orientation relative to the cardiac lumen: parallel (0º – 20º), oblique (20º – 70º), or perpendicular (70º – 90º). **(D-O)** Representative immunofluorescence images of mitotic cells stained against Survivin (green) and SMA (red) in control and *Nrg1*^{flox}*;Tie2*^{Cre} heart sections at E8.5 **(D-I)** and E9.5 **(J-O)**. DAPI counterstaining is shown in blue. White lines indicate the reference plane of the cardiac lumen. Yellow lines indicate the orientation of the mitotic spindle. **(P, Q)** Quantification of OCD at E8.5 and E9.5. *P* values were obtained by Fisher's exact test. **P*-value < 0.05. Scale bar=10 μm.

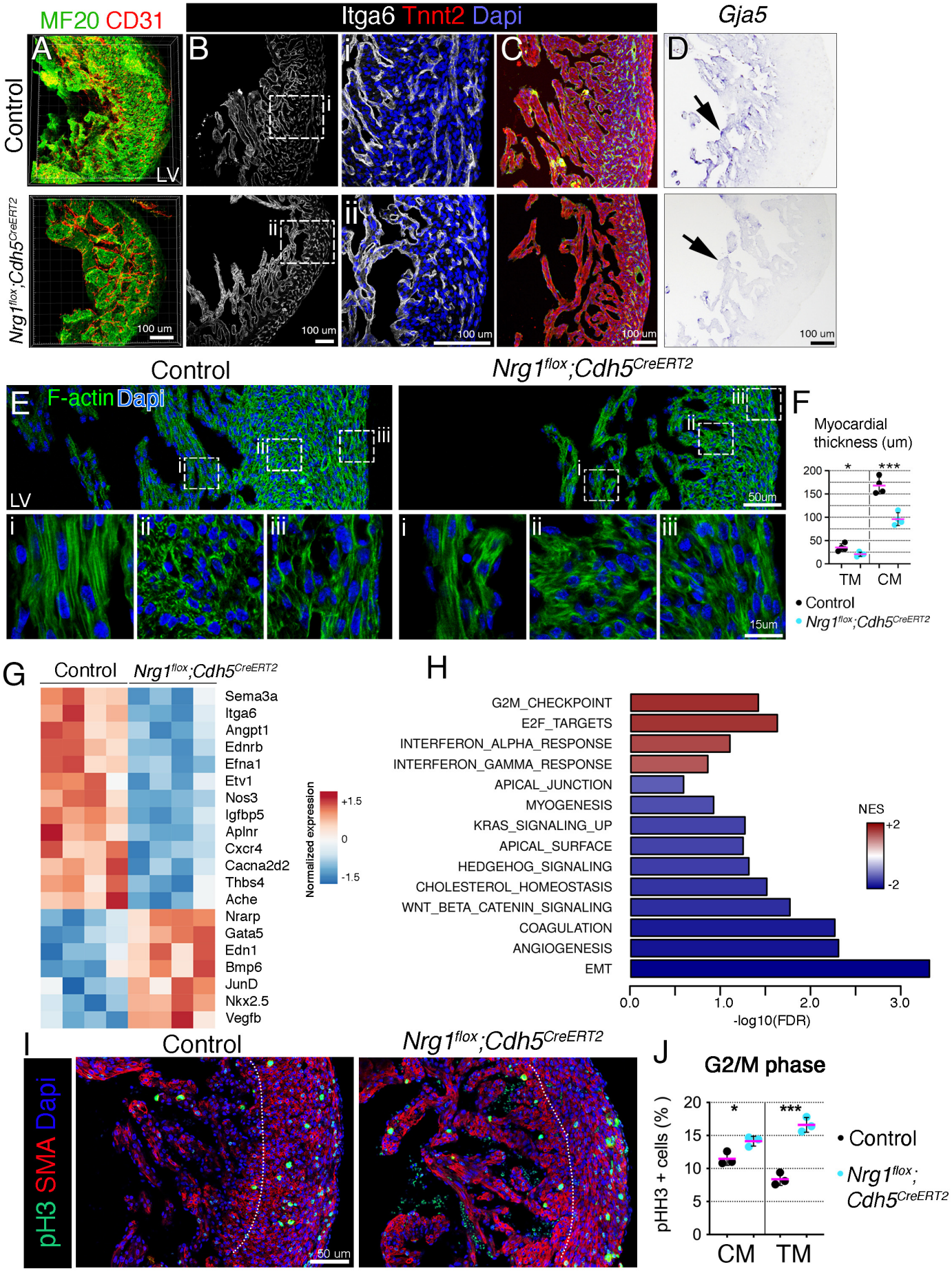

Figure 4_Grego-Bessa

Figure 4. NRG1 is required for inner ventricular wall formation. (A) 3D reconstruction (100µm; Z-stack=50 µm) of MF20 (green) and CD31 (red) whole mount immunofluorescence in E16.5 control and *Nrg1*^{flox}*;Cdh5*^{Cre} hearts after tamoxifen induction at E10.5 and E11.5. **(B,C)** Immunofluorescence against integrin α6 **(B)** and Troponin T2, Tnnt2 (C) in control and *Nrg1*^{flox}*;Cdh5*^{CreERT2} heart transverse sections at E16.5. **(D)** ISH of *Gja5* in E16.5 control and *Nrg1*^{flox}*;Cdh5*^{CreERT2} embryos. Arrows mark trabecular myocardium. **(E)** Phalloidin staining in E16.5 control and *Nrg1*^{flox}*;Cdh5*^{CreERT2} heart sections. **(F)** Quantification of compact and trabecular myocardial thickness (n ≥3). **(G)** Heatmap of representative DEGs in E15.5 control vs. *Nrg1*^{flox}*;Cdh5*^{CreERT2} heart expression profiles. The color code represents normalized gene expression from -1.5 to 1.5. **(H)** GSEA for E15.5 *Nrg1*^{flox}*;Cdh5*^{CreERT2} vs. Control, against Hallmark gene sets. The bar plot represents enrichment data for 14 Hallmark gene sets at FDR qval < 0.25. Of these, 7 had FDR qval < 0.05. Scale bar indicates normalized enrichment score (NES) from -2 to 2. Positive (red) and negative (blue) scores, indicating enrichment or depletion, were found for 4 and 10 gene sets, respectively. **(I)** Phospho-histone 3 (pH3) immunofluorescence on sections of E16.5 control hearts (n=3) and *Nrg1*^{flox}*;Cdh5*^{CreERT2} hearts (n=3). Dotted lines demark the separation between compact and trabecular myocardium. **(J)** Quantification of pH3-positive myocardial cells. **P*-value < 0.05, *** *P* < 0.001, ns= non-significant by Student t-test. Scale bars=100 µm (A-D); 50 µm (E,I); 15µm (E insets).

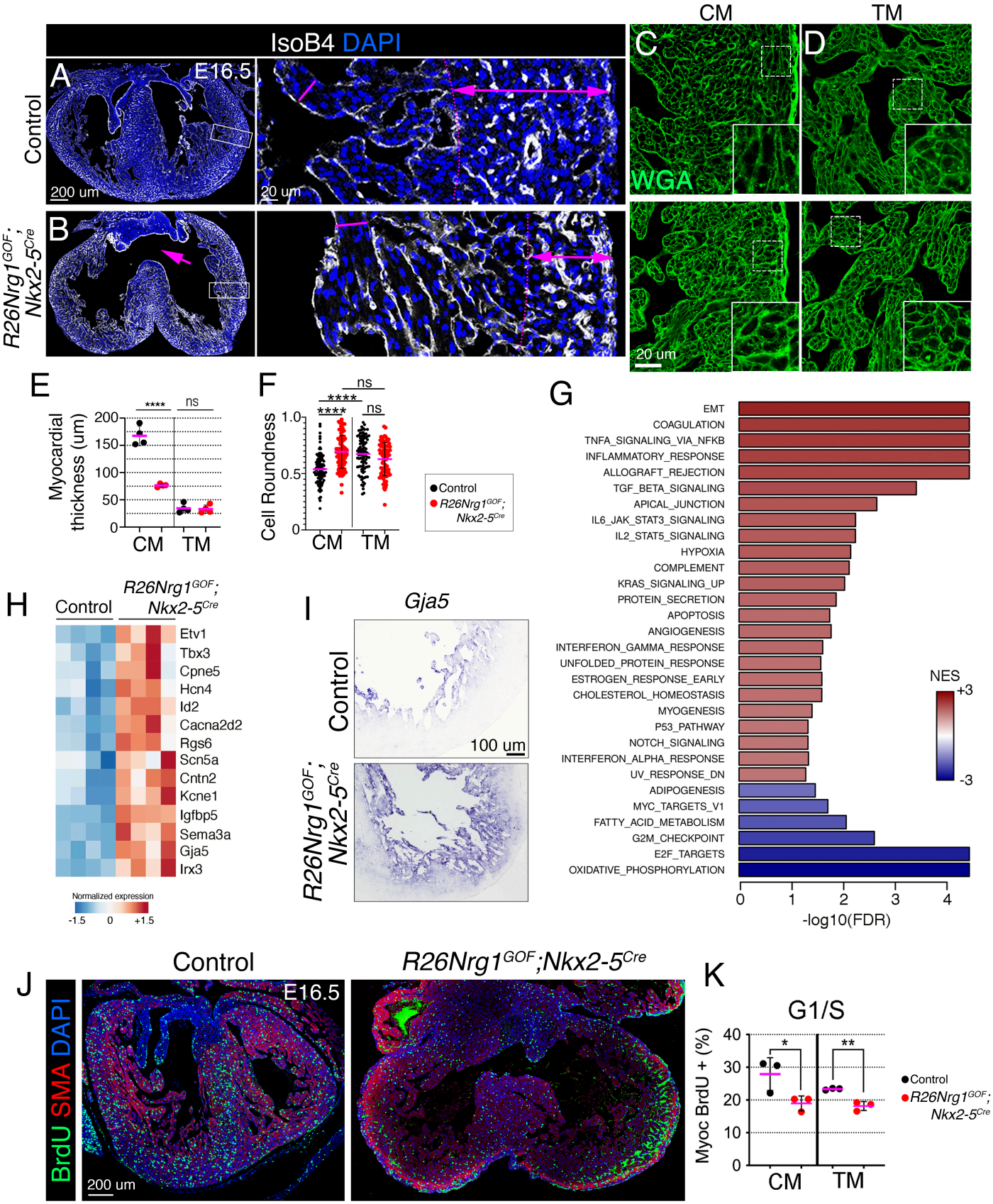

Figure 5_Grego-Bessa

Figure 5. Ectopic NRG1 expression trabeculates myocardium and arrests cardiac development. **(A,B)** DAPI staining in transverse sections of E16.5 control hearts **(A)** and *R26Nrg1^{GOF};Nkx2-5^{Cre}* hearts **(B)**. The arrow in B marks a septal defect. Double-headed arrows in the high-magnification views indicate myocardium thickness. Dotted lines demark the separation between compact myocardium (CM) and trabecular myocardium (TM). **(C,D)** WGA-FITC staining on transverse sections of CM **(C)** and TM **(D)** in E16.5 control and *R26Nrg1^{GOF};Nkx2-5^{Cre}* hearts. **(E)** Quantification of CM and TM thickness in E16.5 control and *R26Nrg1^{GOF};Nkx2-5^{Cre}* (n=3 per genotype) heart sections. **(F)** Quantification of CM and TM cell roundness in E16.5 control and *R26Nrg1^{GOF};Nkx2-5^{Cre}* heart sections (n=3 per genotype). **(G)** GSEA for E15.5 *R26Nrg1^{GOF};Nkx2-5^{Cre}* vs. Control, against Hallmark gene sets. The bar plot represents enrichment data for 30 gene sets at FDR qval < 0.05. Scale bar indicates normalized enrichment score (NES) from -3 to $\pm$3. Positive (red) and negative (blue) scores, indicating enrichment or depletion, were found for 24 and 6 gene sets, respectively. Relative expression values for the "leading edge" genes associated to gene sets EMT and G2/M CHECKPOINT are presented as heatmaps in figure S11. (**H)** Heatmap of representative DEGs in E15.5 *R26Nrg1^{GOF};Nkx2-5^{Cre}* vs. control heart expression profiles. The color code represents normalized gene expression from -1.5 to 1.5. **(I)** ISH for *Gja5* in E16.5 control and *R26Nrg1^{GOF};Nkx2-5^{Cre}* heart sections. **(J)** BrdU immunodetection in E16.5 control and *R26Nrg1^{GOF};Nkx2-5^{Cre}* heart sections. **(K)** Quantification of BrdU incorporation in CM and TM in control and *R26Nrg1^{GOF};Nkx2-5^{Cre}* embryos (n=3 per genotype). *$P < 0.05$, ** $P < 0.01$, **** $P < 0.000$, ns= non-significant by Student t-test. Scale bars= 200 µm (A,B,J); 20 µm (C).

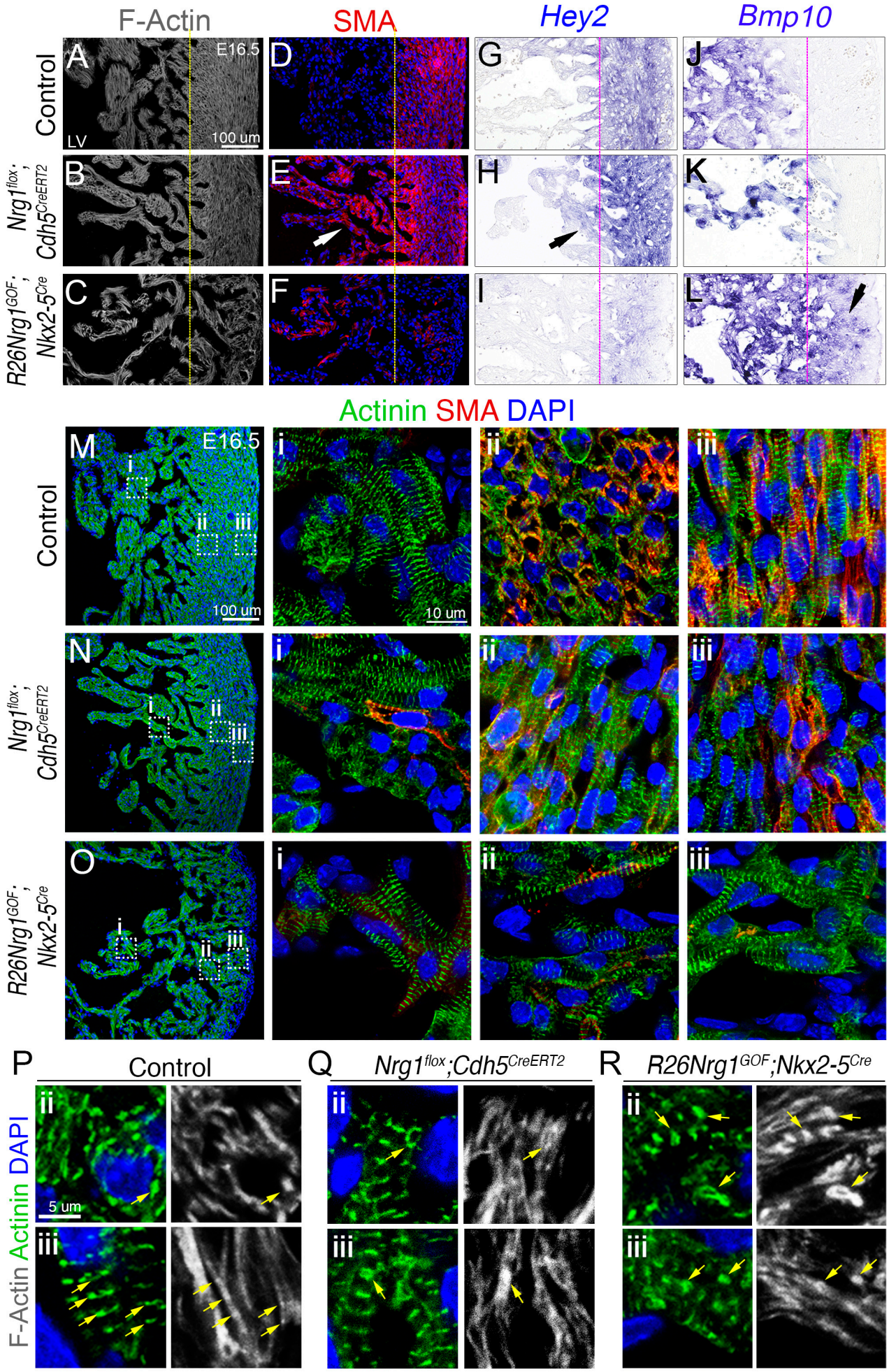

Figure 6_Grego-Bessa

Figure 6. Ventricular patterning is mediated by cytoskeletal dynamics. (A-F) Phalloidin (F-actin) staining and immunofluorescence against smooth muscle actin (SMA) in E16.5 left ventricular sections from control **(A, D)**, *Nrg1*^{flox}*;Cdh5*^{CreERT2} **(B, E)**, and *R26Nrg1*^{GOF}*;Nkx2-5*^{Cre} hearts **(C, F)** . Yellow lines mark the position of the morphological border between trabecular myocardium (TM) and compact myocardium (CM) in control heart sections, showing how this border shifts in *Nrg1*^{flox}*;Cdh5*^{CreERT2} and *R26Nrg1*^{GOF}*;Nkx2-5*^{Cre} hearts. The arrow marks strong SMA immunostaining in TM relative to CM in the *Nrg1*^{flox}*;Cdh5*^{Cre} heart. Note also the reduced SMA expression in CM of *R26Nrg1*^{GOF}*;Nkx2-5*^{Cre} hearts **(F). (G-L)** ISH for *Hey2* and *BMP10* in E16.5 left ventricular sections from control **(G, J)**, *Nrg1*^{flox}*;Cdh5*^{CreERT2} **(H, K)**, and *R26Nrg1*^{GOF}*;Nkx2-5-Cre* hearts **(I, L)**. Pink lines demark the position of the morphological border between TM and CM in control heart sections, showing how this border shifts in *Nrg1*^{flox}*;Cdh5*^{CreERT2} and *R26Nrg1*^{GOF}*;Nkx2-5*^{Cre} hearts. Arrows mark ectopic expression of *Hey2* and *Bmp10* in *Nrg1*^{flox}*;Cdh5*^{CreERT2} and *R26Nrg1*^{GOF}*;Nkx2-5*^{Cre} hearts, respectively. Note also the reduced *Hey2* expression in CM of *R26Nrg1*^{GOF}*;Nkx2-5*^{Cre} hearts (**I**). **(M-O)** Actinin and SMA immunostaining in heart sections from E16.5 control **(M)**, *Nrg1*^{flox}*;Cdh5*^{CreERT2} **(N)**, and *R26Nrg1*^{GOF}*;Nkx2-5*^{Cre} embryos **(O)**. Panels i, ii, and iii show high-magnification views of TM, inner CM, and outer CM, respectively. **(P-R)** Detail of F-actin and actinin double immunofluorescence at E16.5 in inner CM (ii) and outer CM (iii). Yellow arrows mark Z-bands and highlight aberrant Z-band structures in *Nrg1*^{flox}*;Cdh5*^{CreERT2} and *R26Nrg1*^{GOF}*;Nkx2-5*^{Cre} hearts. Scale bars=100 µm (A-O); 10µm (M-O insets i , ii and iii); 5µm (P-R panels ii and iii).

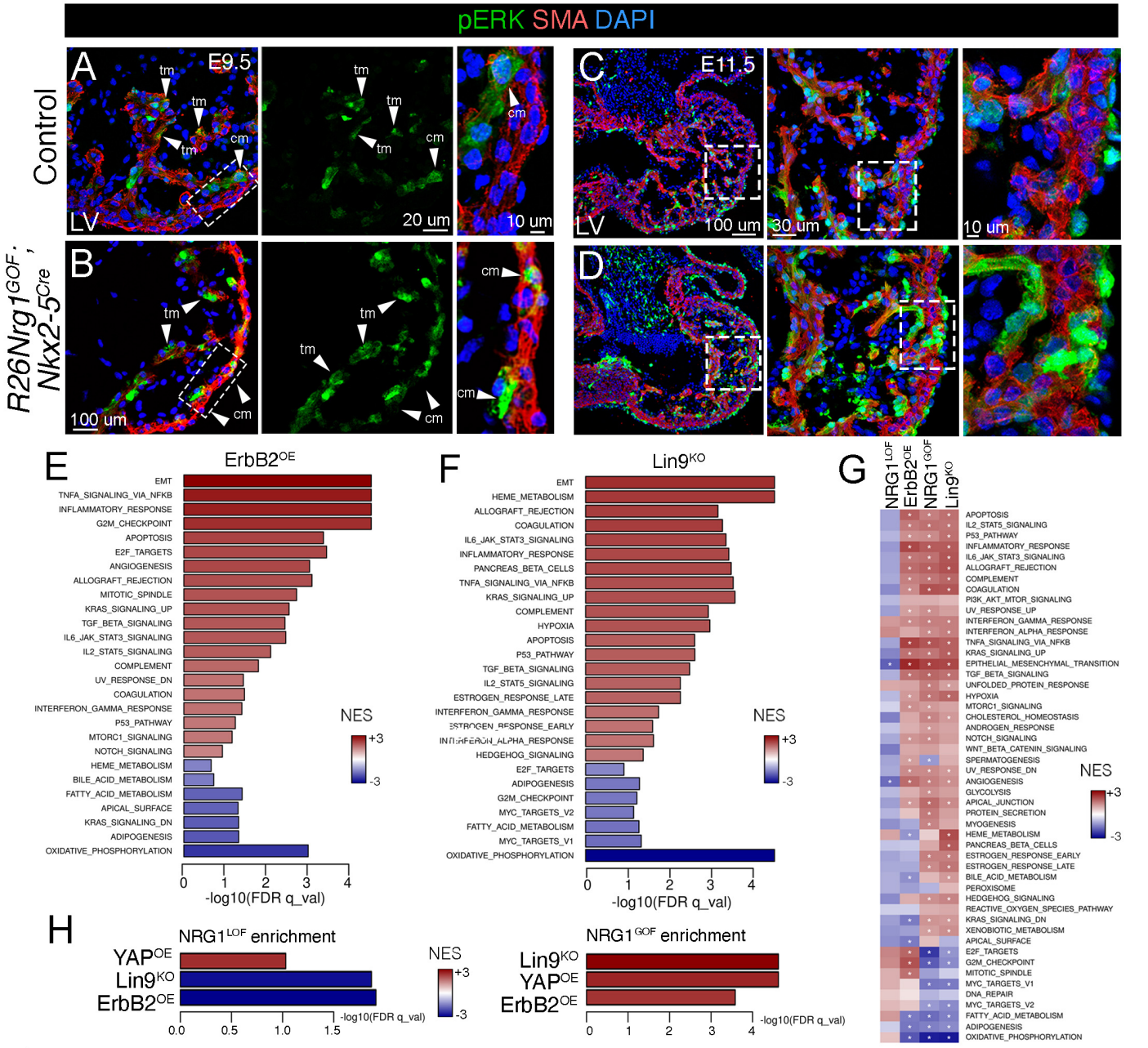

Figure 7_Grego-Bessa

Figure 7. Ectopic pERK expression in *R26Nrg1^{GOF};Nkx2-5^{Cre}* compact myocardium and NRG1-dependent pYAP1 S274 regulation during trabeculation. (A-C) Immunofluorescence for pERK in left ventricular sections from E9.5 **(A, B)** and E11.5 embryos **(C, D)**. Arrowheads mark labeled cardiomyocytes in TM and CM. **(E)** GSEA for ERBB2^{OE} vs. Control [77], against Hallmark gene sets. The barplot represents enrichment data for 27 gene sets at FDR qval < 0.25. Scale bar indicates normalized enrichment score (NES) from -3 to ±3. **(F)** GSEA for LIN9KO vs. Control [78], against Hallmark gene sets. The barplot represents enrichment data for 27 gene sets at FDR qval < 0.25. Scale bar indicates NES from -3 to ±3. **(G)** Comparative heatmap summarizing GSEA results for four genotypes analyzed by RNA-seq (indicated at the top of the heatmap) vs. the corresponding controls. Blue to red colors in scale bar indicate negative to positive NES values. White asterisks indicate gene set enrichment with FDR qval<0.25. **(H)** GSEA for E15.5 *Nrg1^{flox};Cdh5^{CreERT2}* vs. Control (left side) and E15.5 *R26Nrg1^{GOF};Nkx2-5^{Cre}* vs. Control (right side), against gene sets consisting of collections of differentially expressed genes derived from ERBB2^{OE} vs. Control [77] and LIN9KO vs. Control [78], or direct YAP1-target genes [80]. The barplots represent enrichment data at FDR qval < 0.25, and the scale bar indicates normalized enrichment score (NES) from -3 to 3. **(I, J)** Immunofluorescence against pYAP S274 in E9.5 control and *Nrg1^{flox};Tie2^{Cre}* heart sections. Arrows mark cytoplasmic signal, arrowheads nuclear signal. **(K)** Western blot analysis of pYAP S274 and pMOB1 Thr35 in E9.5 control and *Nrg1^{flox};Tie2^{Cre}* ventricles (pool of n=3 per genotype). **(L, N)** Western blot analysis of pYAP S274, pERK 42/44, and pMOB1 Thr35 in E16.5 control, *Nrg1^{flox};Cdh5^{CreERT2}*, and *R26Nrg1^{GOF};Nkx2-5^{Cre}* ventricles (n=1 per genotype). α−Tubulin was used as a gel-loading control. **(N-P)** Immunofluorescence against pYAP S274 on E16.5 control, *Nrg1^{flox};Cdh5^{CreERT2}*, and *R26Nrg1^{GOF};Nkx2-5^{Cre}* heart sections. Arrows mark non-mitotic nuclei, arrowheads mitotic nuclei. LV, left ventricle. Scale bars= (A, B) 100 μm, 20 μm, and 10 μm from low to high magnification view; (C, D) 100 μm, 30 μm, and 10 μm; (I,J) 50 μm; (I,J i,ii) 10 μm; (N-P) 50 μm.

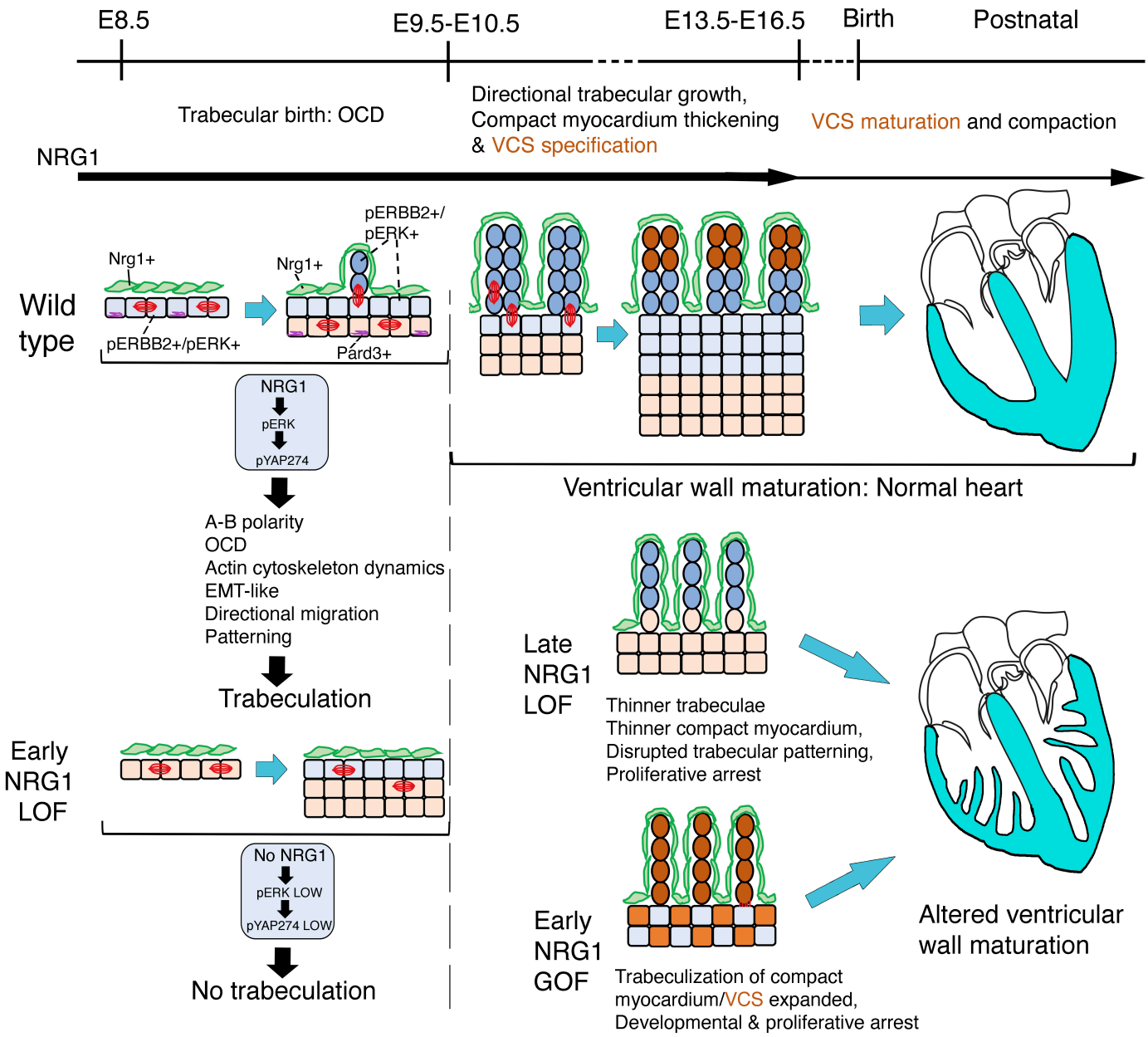

Figure 8_Grego-Bessa et al

Figure 8. NRG1 regulates cardiomyocyte dynamics, proliferation, and maturation during ventricular chamber morphogenesis. Wild-type (E8.5-E10.5): Early trabeculae emerge from a bi-layered myocardium when NRG1 released from the endocardium (cells in green) activates pERBB2 and pERK in the adjacent inner myocardial layer (cells in blue). NRG1-ERBB2-pERK signaling promotes pYAP S274 nuclear localization, and is associated with maintenance of apico-basal (A-B) polarity and parallel divisions in the outer myocardial layer and perpendicular oriented cell divisions (OCD) in the inner myocardial layer, activation of actin cytoskeleton dynamics, cellular migration, and chamber patterning (compact vs. trabecular). **LOF (E8.5-E10.5):** Deficient NRG1 signaling leads to a reduction of perpendicular divisions in favor of parallel divisions (impaired OCD), causing aberrant thickening of the compact layer and lack of trabeculae. These changes are associated with the loss of apico-basal (A-B) polarity markers, disorganized actin cytoskeleton, absence of pERK activation, and inhibition of pYAP S274 nuclear localization. **Wild-type (E10.5-E13-5):** Trabeculae elongate by directional migration from the outer layer compact myocardium, which grows by proliferation. NRG1 is required for specification of the ventricular conduction system (VCS) in trabeculae (brown cells) but is not required for compaction in late gestation or postnatally. **LOF (E10.5-E16.5):** Upon NRG1 inactivation, trabeculae express compact myocardium genes, leading to trabecular mis-patterning, the absence of an inner myocardial wall, and impaired trabecular elongation. **GOF (E10.5-E16.5):** Cardiac NRG1 overexpression induces ectopic trabecular marker expression and trabeculation of the compact myocardium. Cardiomyocyte proliferation is arrested and VCS gene expression expanded, while excessive proliferation of endothelial and epicardial cells alters the cell composition of the ventricular wall. Both NRG1 LOF and GOF lead to failed ventricular chamber maturation and cardiac developmental arrest.

References

1. Jimenez-Amilburu V, Rasouli SJ, Staudt DW, Nakajima H, Chiba A, Mochizuki N, Stainier DY. In Vivo Visualization of Cardiomyocyte Apicobasal Polarity Reveals Epithelial to Mesenchymal-like Transition during Cardiac Trabeculation. *Cell Rep.* 2016;17:2687-2699.

2. Lee J, Vedula V, Baek KI, Chen J, Hsu JJ, Ding Y, Chang CC, Kang H, Small A, Fei P, Chuong CM, Li R, Demer L, Packard RRS, Marsden AL, Hsiai TK. Spatial and temporal variations in hemodynamic forces initiate cardiac trabeculation. *JCI Insight.* 2018;3.

3. Liu J, Bressan M, Hassel D, Huisken J, Staudt D, Kikuchi K, Poss KD, Mikawa T, Stainier DY. A dual role for ErbB2 signaling in cardiac trabeculation. *Development.* 2010;137:3867-3875.

4. Peshkovsky C, Totong R, Yelon D. Dependence of cardiac trabeculation on neuregulin signaling and blood flow in zebrafish. *Dev Dyn.* 2011;240:446-456.

5. Priya R, Allanki S, Gentile A, Mansingh S, Uribe V, Maischein HM, Stainier DYR. Tension heterogeneity directs form and fate to pattern the myocardial wall. *Nature.* 2020;588:130-134.

6. Li J, Miao L, Shieh D, Spiotto E, Li J, Zhou B, Paul A, Schwartz RJ, Firulli AB, Singer HA, Huang G, Wu M. Single-Cell Lineage Tracing Reveals that Oriented Cell Division Contributes to Trabecular Morphogenesis and Regional Specification. *Cell Rep.* 2016;15:158-170.

7. Miao L, Li J, Li J, Lu Y, Shieh D, Mazurkiewicz JE, Barroso M, Schwarz JJ, Xin HB, Singer HA, Vincent PA, Zhong W, Radice GL, Wan LQ, Fan ZC, Huang G, Wu M. Cardiomyocyte orientation modulated by the Numb family proteins-N-cadherin axis is essential for ventricular wall morphogenesis. *Proc Natl Acad Sci U S A.* 2019;116:15560-15569.

8. Yue Y, Zong W, Li X, Li J, Zhang Y, Wu R, Liu Y, Cui J, Wang Q, Bian Y, Yu X, Liu Y, Tan G, Zhang Y, Zhao G, Zhou B, Chen L, Xiao W, Cheng H, He A. Long-term, in toto live imaging of cardiomyocyte behaviour during mouse ventricle chamber formation at single-cell resolution. *Nat Cell Biol.* 2020;22:332-340.

9. Sedmera D, Pexieder T, Vuillemin M, Thompson RP, Anderson RH. Developmental patterning of the myocardium. *Anat Rec.* 2000;258:319-337.

10. Gourdie RG, Mima T, Thompson RP, Mikawa T. Terminal diversification of the myocyte lineage generates Purkinje fibers of the cardiac conduction system. *Development.* 1995;121:1423-1431.

11. Moorman AF, Christoffels VM. Cardiac chamber formation: development, genes, and evolution. *Physiol Rev.* 2003;83:1223-1267.

12. Tian X, Hu T, Zhang H, He L, Huang X, Liu Q, Yu W, He L, Yang Z, Yan Y, Yang X, Zhong TP, Pu WT, Zhou B. Vessel formation. De novo formation of a distinct coronary vascular population in neonatal heart. *Science.* 2014;345:90-94.

13. Tian X, Li Y, He L, Zhang H, Huang X, Liu Q, Pu W, Zhang L, Li Y, Zhao H, Wang Z, Zhu J, Nie Y, Hu S, Sedmera D, Zhong TP, Yu Y, Zhang L, Yan Y, Qiao Z, Wang QD, Wu SM, Pu WT, Anderson RH, Zhou B. Identification of a hybrid myocardial zone in the mammalian heart after birth. *Nat Commun.* 2017;8:87.

14. Wu B, Zhang Z, Lui W, Chen X, Wang Y, Chamberlain AA, Moreno-Rodriguez RA, Markwald RR, O'Rourke BP, Sharp DJ, Zheng D, Lenz J, Baldwin HS, Chang CP, Zhou B. Endocardial cells form the coronary arteries by angiogenesis through myocardial-endocardial VEGF signaling. *Cell.* 2012;151:1083-1096.

15. Choquet C, Kelly RG, Miquerol L. Defects in Trabecular Development Contribute to Left Ventricular Noncompaction. *Pediatr Cardiol.* 2019;40:1331-1338.

16. Finsterer J, Stollberger C, Towbin JA. Left ventricular noncompaction cardiomyopathy: cardiac, neuromuscular, and genetic factors. *Nat Rev Cardiol.* 2017;14:224-237.

17. Arbustini E, Weidemann F, Hall JL. Left ventricular noncompaction: a distinct cardiomyopathy or a trait shared by different cardiac diseases? *J Am Coll Cardiol.* 2014;64:1840-1850.

18. Abela M, D'Silva A. Left Ventricular Trabeculations in Athletes: Epiphenomenon or Phenotype of Disease? *Curr Treat Options Cardiovasc Med.* 2018;20:100.

19. Meyer HV, Dawes TJW, Serrani M, Bai W, Tokarczuk P, Cai J, de Marvao A, Henry A, Lumbers RT, Gierten J, Thumberger T, Wittbrodt J, Ware JS, Rueckert D, Matthews PM, Prasad SK, Costantino ML, Cook SA, Birney E, O'Regan DP. Genetic and functional insights into the fractal structure of the heart. *Nature.* 2020;584:589-594.

20. Anderson RH, Jensen B, Mohun TJ, Petersen SE, Aung N, Zemrak F, Planken RN, MacIver DH. Key Questions Relating to Left Ventricular Noncompaction Cardiomyopathy: Is the Emperor Still Wearing Any Clothes? *Can J Cardiol.* 2017;33:747-757.

21. Oechslin E, Jenni R, Klaassen S. Left Ventricular Noncompaction Is a Myocardial Phenotype: Cardiomyopathy-Yes or No? *Can J Cardiol.* 2021;37:366-369.

22. Weir-McCall JR, Yeap PM, Papagiorcopulo C, Fitzgerald K, Gandy SJ, Lambert M, Belch JJ, Cavin I, Littleford R, Macfarlane JA, Matthew SZ, Nicholas RS, Struthers AD, Sullivan F, Waugh SA, White RD, Houston JG. Left Ventricular Noncompaction: Anatomical Phenotype or Distinct Cardiomyopathy? *J Am Coll Cardiol.* 2016;68:2157-2165.

23. Lai D, Liu X, Forrai A, Wolstein O, Michalicek J, Ahmed I, Garratt AN, Birchmeier C, Zhou M, Hartley L, Robb L, Feneley MP, Fatkin D, Harvey RP. Neuregulin 1 sustains the gene regulatory network in both trabecular and nontrabecular myocardium. *Circ Res.* 2010;107:715-727.

24. Meyer D, Birchmeier C. Multiple essential functions of neuregulin in development. *Nature.* 1995;378:386-390.

25. Rasouli SJ, Stainier DYR. Regulation of cardiomyocyte behavior in zebrafish trabeculation by Neuregulin 2a signaling. *Nat Commun.* 2017;8:15281.

26. Sanchez-Soria P, Camenisch TD. ErbB signaling in cardiac development and disease. *Semin Cell Dev Biol.* 2010;21:929-935.

27. Baliga RR, Pimental DR, Zhao YY, Simmons WW, Marchionni MA, Sawyer DB, Kelly RA. NRG-1-induced cardiomyocyte hypertrophy. Role of PI-3-kinase, p70(S6K), and MEK-MAPK-RSK. *Am J Physiol.* 1999;277:H2026-2037.

28. Del Monte-Nieto G, Ramialison M, Adam AAS, Wu B, Aharonov A, D'Uva G, Bourke LM, Pitulescu ME, Chen H, de la Pompa JL, Shou W, Adams RH, Harten SK, Tzahor E, Zhou B, Harvey RP. Control of cardiac jelly dynamics by NOTCH1 and NRG1 defines the building plan for trabeculation. *Nature.* 2018;557:439-445.

29. Gassmann M, Casagranda F, Orioli D, Simon H, Lai C, Klein R, Lemke G. Aberrant neural and cardiac development in mice lacking the ErbB4 neuregulin receptor. *Nature.* 1995;378:390-394.

30. Kramer R, Bucay N, Kane DJ, Martin LE, Tarpley JE, Theill LE. Neuregulins with an Ig-like domain are essential for mouse myocardial and neuronal development. *Proc Natl Acad Sci U S A.* 1996;93:4833-4838.

31. Lai JKH, Collins MM, Uribe V, Jimenez-Amilburu V, Gunther S, Maischein HM, Stainier DYR. The Hippo pathway effector Wwtr1 regulates cardiac wall maturation in zebrafish. *Development.* 2018;145.

32. Lee KF, Simon H, Chen H, Bates B, Hung MC, Hauser C. Requirement for neuregulin receptor erbB2 in neural and cardiac development. *Nature.* 1995;378:394-398.

33. Bersell K, Arab S, Haring B, Kuhn B. Neuregulin1/ErbB4 signaling induces cardiomyocyte proliferation and repair of heart injury. *Cell.* 2009;138:257-270.

34. D'Uva G, Aharonov A, Lauriola M, Kain D, Yahalom-Ronen Y, Carvalho S, Weisinger K, Bassat E, Rajchman D, Yifa O, Lysenko M, Konfino T, Hegesh J, Brenner O, Neeman M, Yarden Y, Leor J, Sarig R, Harvey RP, Tzahor E. ERBB2 triggers mammalian heart regeneration by promoting cardiomyocyte dedifferentiation and proliferation. *Nat Cell Biol.* 2015;17:627-638.

35. Polizzotti BD, Ganapathy B, Walsh S, Choudhury S, Ammanamanchi N, Bennett DG, dos Remedios CG, Haubner BJ, Penninger JM, Kuhn B. Neuregulin stimulation of cardiomyocyte regeneration in mice and human myocardium reveals a therapeutic window. *Sci Transl Med.* 2015;7:281ra245.

36. Liu X, Gu X, Li Z, Li X, Li H, Chang J, Chen P, Jin J, Xi B, Chen D, Lai D, Graham RM, Zhou M. Neuregulin-1/erbB-activation improves cardiac function and survival in models of ischemic, dilated, and viral cardiomyopathy. *J Am Coll Cardiol.* 2006;48:1438-1447.

37. Gao R, Zhang J, Cheng L, Wu X, Dong W, Yang X, Li T, Liu X, Xu Y, Li X, Zhou M. A Phase II, randomized, double-blind, multicenter, based on standard therapy, placebo-controlled study of the efficacy and safety of recombinant human neuregulin-1 in patients with chronic heart failure. *J Am Coll Cardiol.* 2010;55:1907-1914.

38. Jabbour A, Hayward CS, Keogh AM, Kotlyar E, McCrohon JA, England JF, Amor R, Liu X, Li XY, Zhou MD, Graham RM, Macdonald PS. Parenteral administration of recombinant human neuregulin-1 to patients with stable chronic heart failure produces favourable acute and chronic haemodynamic responses. *Eur J Heart Fail.* 2011;13:83-92.

39. Sawyer DB, Caggiano A. Neuregulin-1beta for the treatment of systolic heart failure. *J Mol Cell Cardiol.* 2011;51:501-505.

40. Geissler A, Ryzhov S, Sawyer DB. Neuregulins: protective and reparative growth factors in multiple forms of cardiovascular disease. *Clin Sci (Lond).* 2020;134:2623-2643.

41. Samsa LA, Givens C, Tzima E, Stainier DY, Qian L, Liu J. Cardiac contraction activates endocardial Notch signaling to modulate chamber maturation in zebrafish. *Development.* 2015;142:4080-4091.

42. Yang X, Arber S, William C, Li L, Tanabe Y, Jessell TM, Birchmeier C, Burden SJ. Patterning of muscle acetylcholine receptor gene expression in the absence of motor innervation. *Neuron.* 2001;30:399-410.

43. Kisanuki YY, Hammer RE, Miyazaki J, Williams SC, Richardson JA, Yanagisawa M. Tie2-Cre transgenic mice: a new model for endothelial cell-lineage analysis in vivo. *Dev Biol.* 2001;230:230-242.

44. Fukazawa R, Miller TA, Kuramochi Y, Frantz S, Kim YD, Marchionni MA, Kelly RA, Sawyer DB. Neuregulin-1 protects ventricular myocytes from anthracycline-induced apoptosis via erbB4-dependent activation of PI3-kinase/Akt. *J Mol Cell Cardiol.* 2003;35:1473-1479.

45. Liu FF, Stone JR, Schuldt AJ, Okoshi K, Okoshi MP, Nakayama M, Ho KK, Manning WJ, Marchionni MA, Lorell BH, Morgan JP, Yan X. Heterozygous knockout of neuregulin-1 gene in mice exacerbates doxorubicin-induced heart failure. *Am J Physiol Heart Circ Physiol.* 2005;289:H660-666.

46. Camenisch TD, Schroeder JA, Bradley J, Klewer SE, McDonald JA. Heart-valve mesenchyme formation is dependent on hyaluronan-augmented activation of ErbB2-ErbB3 receptors. *Nat Med.* 2002;8:850-855.

47. Passer D, van de Vrugt A, Atmanli A, Domian IJ. Atypical Protein Kinase C-Dependent Polarized Cell Division Is Required for Myocardial Trabeculation. *Cell Rep.* 2016;14:1662-1672.

48. Li G, Tian L, Goodyer W, Kort EJ, Buikema JW, Xu A, Wu JC, Jovinge S, Wu SM. Single cell expression analysis reveals anatomical and cell cycle-dependent transcriptional shifts during heart development. *Development.* 2019;146.

49. Liberzon A, Birger C, Thorvaldsdottir H, Ghandi M, Mesirov JP, Tamayo P. The Molecular Signatures Database (MSigDB) hallmark gene set collection. *Cell Syst.* 2015;1:417-425.

50. Harris SL, Levine AJ. The p53 pathway: positive and negative feedback loops. *Oncogene.* 2005;24:2899-2908.

51. Staudt DW, Liu J, Thorn KS, Stuurman N, Liebling M, Stainier DY. High-resolution imaging of cardiomyocyte behavior reveals two distinct steps in ventricular trabeculation. *Development.* 2014;141:585-593.

52. Li R, Gundersen GG. Beyond polymer polarity: how the cytoskeleton builds a polarized cell. *Nat Rev Mol Cell Biol.* 2008;9:860-873.

53. Cherian AV, Fukuda R, Augustine SM, Maischein HM, Stainier DY. N-cadherin relocalization during cardiac trabeculation. *Proc Natl Acad Sci U S A.* 2016;113:7569-7574.

54. McCaffrey LM, Macara IG. Signaling pathways in cell polarity. *Cold Spring Harb Perspect Biol.* 2012;4.

55. Hikita T, Mirzapourshafiyi F, Barbacena P, Riddell M, Pasha A, Li M, Kawamura T, Brandes RP, Hirose T, Ohno S, Gerhardt H, Matsuda M, Franco CA, Nakayama M. PAR-3 controls endothelial planar polarity and vascular inflammation under laminar flow. *EMBO Rep.* 2018;19.

56. Jimenez-Amilburu V, Stainier DYR. The transmembrane protein Crb2a regulates cardiomyocyte apicobasal polarity and adhesion in zebrafish. *Development.* 2019;146.

57. Coopman P, Djiane A. Adherens Junction and E-Cadherin complex regulation by epithelial polarity. *Cell Mol Life Sci.* 2016;73:3535-3553.

58. Wang Y, Nakayama M, Pitulescu ME, Schmidt TS, Bochenek ML, Sakakibara A, Adams S, Davy A, Deutsch U, Luthi U, Barberis A, Benjamin LE, Makinen T, Nobes CD, Adams RH. Ephrin-B2 controls VEGF-induced angiogenesis and lymphangiogenesis. *Nature.* 2010;465:483-486.

59. Davenport AP, Hyndman KA, Dhaun N, Southan C, Kohan DE, Pollock JS, Pollock DM, Webb DJ, Maguire JJ. Endothelin. *Pharmacol Rev.* 2016;68:357-418.

60. Ivins S, Chappell J, Vernay B, Suntharalingham J, Martineau A, Mohun TJ, Scambler PJ. The CXCL12/CXCR4 Axis Plays a Critical Role in Coronary Artery Development. *Dev Cell.* 2015;33:455-468.

61. Kwon HB, Wang S, Helker CS, Rasouli SJ, Maischein HM, Offermanns S, Herzog W, Stainier DY. In vivo modulation of endothelial polarization by Apelin receptor signalling. *Nat Commun.* 2016;7:11805.

62. Rasanen M, Sultan I, Paech J, Hemanthakumar KA, Yu W, He L, Tang J, Sun Y, Hlushchuk R, Huan X, Armstrong E, Khoma OZ, Mervaala E, Djonov V, Betsholtz C, Zhou B, Kivela R, Alitalo K. VEGF-B Promotes Endocardium-Derived Coronary Vessel Development and Cardiac Regeneration. *Circulation.* 2021;143:65-77.

63. Suri C, Jones PF, Patan S, Bartunkova S, Maisonpierre PC, Davis S, Sato TN, Yancopoulos GD. Requisite role of angiopoietin-1, a ligand for the TIE2 receptor, during embryonic angiogenesis. *Cell.* 1996;87:1171-1180.

64. Li Y, Tian X, Zhao H, He L, Zhang S, Huang X, Zhang H, Miquerol L, Zhou B. Genetic targeting of Purkinje fibres by Sema3a-CreERT2. *Sci Rep.* 2018;8:2382.

65. Klein R. Eph/ephrin signalling during development. *Development.* 2012;139:4105-4109.

66. Munshi NV. Gene regulatory networks in cardiac conduction system development. *Circ Res.* 2012;110:1525-1537.

67. Shekhar A, Lin X, Liu FY, Zhang J, Mo H, Bastarache L, Denny JC, Cox NJ, Delmar M, Roden DM, Fishman GI, Park DS. Transcription factor ETV1 is essential for rapid conduction in the heart. *J Clin Invest.* 2016;126:4444-4459.

68. Sun Q, Liu S, Liu K, Jiao K. Role of Semaphorin Signaling During Cardiovascular Development. *J Am Heart Assoc.* 2018;7.

69. Travisano SI, Oliveira VL, Prados B, Grego-Bessa J, Pineiro-Sabaris R, Bou V, Gomez MJ, Sanchez-Cabo F, MacGrogan D, de la Pompa JL. Coronary arterial development is regulated by a Dll4-Jag1-EphrinB2 signaling cascade. *Elife.* 2019;8:1-30.

70. Claxton S, Kostourou V, Jadeja S, Chambon P, Hodivala-Dilke K, Fruttiger M. Efficient, inducible Cre-recombinase activation in vascular endothelium. *Genesis.* 2008;46:74-80.

71. Sharma B, Ho L, Ford GH, Chen HI, Goldstone AB, Woo YJ, Quertermous T, Reversade B, Red-Horse K. Alternative Progenitor Cells Compensate to Rebuild the Coronary Vasculature in Elabela- and Apj-Deficient Hearts. *Dev Cell.* 2017;42:655-666 e653.

72. Haskins JW, Nguyen DX, Stern DF. Neuregulin 1-activated ERBB4 interacts with YAP to induce Hippo pathway target genes and promote cell migration. *Sci Signal.* 2014;7:ra116.

73. Hertig V, Matos-Nieves A, Garg V, Villeneuve L, Mamarbachi M, Caland L, Calderone A. Nestin expression is dynamically regulated in cardiomyocytes during embryogenesis. *J Cell Physiol.* 2018;233:3218-3229.

74. Goodyer WR, Beyersdorf BM, Paik DT, Tian L, Li G, Buikema JW, Chirikian O, Choi S, Venkatraman S, Adams EL, Tessier-Lavigne M, Wu JC, Wu SM. Transcriptomic Profiling of the Developing Cardiac Conduction System at Single-Cell Resolution. *Circ Res.* 2019;125:379-397.

75. Rentschler S, Zander J, Meyers K, France D, Levine R, Porter G, Rivkees SA, Morley GE, Fishman GI. Neuregulin-1 promotes formation of the murine cardiac conduction system. *Proc Natl Acad Sci U S A.* 2002;99:10464-10469.

76. Ya J, Markman MW, Wagenaar GT, Blommaart PJ, Moorman AF, Lamers WH. Expression of the smooth-muscle proteins alpha-smooth-muscle actin and calponin, and of the intermediate filament protein desmin are parameters of cardiomyocyte maturation in the prenatal rat heart. *Anat Rec.* 1997;249:495-505.

77. Aharonov A, Shakked A, Umansky KB, Savidor A, Genzelinakh A, Kain D, Lendengolts D, Revach OY, Morikawa Y, Dong J, Levin Y, Geiger B, Martin JF, Tzahor E. ERBB2 drives YAP activation and EMT-like processes during cardiac regeneration. *Nat Cell Biol.* 2020;22:1346-1356.

78. Grundl M, Walz S, Hauf L, Schwab M, Werner KM, Spahr S, Schulte C, Maric HM, Ade CP, Gaubatz S. Interaction of YAP with the Myb-MuvB (MMB) complex defines a transcriptional program to promote the proliferation of cardiomyocytes. *PLoS Genet.* 2020;16:e1008818.

79. Pattschull G, Walz S, Grundl M, Schwab M, Ruhl E, Baluapuri A, Cindric-Vranesic A, Kneitz S, Wolf E, Ade CP, Rosenwald A, von Eyss B, Gaubatz S. The Myb-MuvB Complex Is Required for YAP-Dependent Transcription of Mitotic Genes. *Cell Rep.* 2019;27:3533-3546 e3537.

80. Monroe TO, Hill MC, Morikawa Y, Leach JP, Heallen T, Cao S, Krijger PHL, de Laat W, Wehrens XHT, Rodney GG, Martin JF. YAP Partially Reprograms Chromatin Accessibility to Directly Induce Adult Cardiogenesis In Vivo. *Dev Cell.* 2019;48:765-779 e767.

81. Yang S, Zhang L, Liu M, Chong R, Ding SJ, Chen Y, Dong J. CDK1 phosphorylation of YAP promotes mitotic defects and cell motility and is essential for neoplastic transformation. *Cancer Res.* 2013;73:6722-6733.

82. Vlahov N, Scrace S, Soto MS, Grawenda AM, Bradley L, Pankova D, Papaspyropoulos A, Yee KS, Buffa F, Goding CR, Timpson P, Sibson N, O'Neill E. Alternate RASSF1 Transcripts Control SRC Activity, E-Cadherin Contacts, and YAP-Mediated Invasion. *Curr Biol.* 2015;25:3019-3034.

83. Gupta V, Poss KD. Clonally dominant cardiomyocytes direct heart morphogenesis. *Nature.* 2012;484:479-484.

84. di Pietro F, Echard A, Morin X. Regulation of mitotic spindle orientation: an integrated view. *EMBO Rep.* 2016;17:1106-1130.

85. Nelson WJ. Adaptation of core mechanisms to generate cell polarity. *Nature.* 2003;422:766-774.

86. Meilhac SM, Kelly RG, Rocancourt D, Eloy-Trinquet S, Nicolas JF, Buckingham ME. A retrospective clonal analysis of the myocardium reveals two phases of clonal growth in the developing mouse heart. *Development.* 2003;130:3877-3889.

87. Ong LL, Kim N, Mima T, Cohen-Gould L, Mikawa T. Trabecular myocytes of the embryonic heart require N-cadherin for migratory unit identity. *Dev Biol.* 1998;193:1-9.

88. Yang J, Antin P, Berx G, Blanpain C, Brabletz T, Bronner M, Campbell K, Cano A, Casanova J, Christofori G, Dedhar S, Derynck R, Ford HL, Fuxe J, Garcia de Herreros A, Goodall GJ, Hadjantonakis AK, Huang RYJ,

Kalcheim C, Kalluri R, Kang Y, Khew-Goodall Y, Levine H, Liu J, Longmore GD, Mani SA, Massague J, Mayor R, McClay D, Mostov KE, Newgreen DF, Nieto MA, Puisieux A, Runyan R, Savagner P, Stanger B, Stemmler MP, Takahashi Y, Takeichi M, Theveneau E, Thiery JP, Thompson EW, Weinberg RA, Williams ED, Xing J, Zhou BP, Sheng G, Association EMTI. Guidelines and definitions for research on epithelial-mesenchymal transition. *Nat Rev Mol Cell Biol.* 2020;21:341-352.

89. Barak Y, Hemberger M, Sucov HM. Phases and Mechanisms of Embryonic Cardiomyocyte Proliferation and Ventricular Wall Morphogenesis. *Pediatr Cardiol.* 2019;40:1359-1366.

90. Cao Y, Duca S, Cao J. Epicardium in Heart Development. *Cold Spring Harb Perspect Biol.* 2020;12.

91. Quijada P, Trembley MA, Small EM. The Role of the Epicardium During Heart Development and Repair. *Circ Res.* 2020;126:377-394.

92. Batlle E, Wilkinson DG. Molecular mechanisms of cell segregation and boundary formation in development and tumorigenesis. *Cold Spring Harb Perspect Biol.* 2012;4:a008227.

93. Friedl P, Gilmour D. Collective cell migration in morphogenesis, regeneration and cancer. *Nat Rev Mol Cell Biol.* 2009;10:445-457.

94. LeGoff L, Lecuit T. Mechanical Forces and Growth in Animal Tissues. *Cold Spring Harb Perspect Biol.* 2015;8:a019232.

95. Lim HYG, Plachta N. Cytoskeletal control of early mammalian development. *Nat Rev Mol Cell Biol.* 2021;22:548-562.

96. Ruijtenberg S, van den Heuvel S. Coordinating cell proliferation and differentiation: Antagonism between cell cycle regulators and cell type-specific gene expression. *Cell Cycle.* 2016;15:196-212.

97. de Gooijer MC, van den Top A, Bockaj I, Beijnen JH, Wurdinger T, van Tellingen O. The G2 checkpoint-a node-based molecular switch. *FEBS Open Bio.* 2017;7:439-455.

98. Musacchio A, Salmon ED. The spindle-assembly checkpoint in space and time. *Nat Rev Mol Cell Biol.* 2007;8:379-393.

99. Nakaseko Y, Yanagida M. Cell biology. Cytoskeleton in the cell cycle. *Nature.* 2001;412:291-292.

100. Giono LE, Manfredi JJ. The p53 tumor suppressor participates in multiple cell cycle checkpoints. *J Cell Physiol.* 2006;209:13-20.

101. Cho RJ, Campbell MJ, Winzeler EA, Steinmetz L, Conway A, Wodicka L, Wolfsberg TG, Gabrielian AE, Landsman D, Lockhart DJ, Davis RW. A

genome-wide transcriptional analysis of the mitotic cell cycle. *Mol Cell.* 1998;2:65-73.

102. Ishida S, Huang E, Zuzan H, Spang R, Leone G, West M, Nevins JR. Role for E2F in control of both DNA replication and mitotic functions as revealed from DNA microarray analysis. *Mol Cell Biol.* 2001;21:4684-4699.

103. Matsumura I, Tanaka H, Kanakura Y. E2F1 and c-Myc in cell growth and death. *Cell Cycle.* 2003;2:333-338.

104. Jones MC, Zha J, Humphries MJ. Connections between the cell cycle, cell adhesion and the cytoskeleton. *Philos Trans R Soc Lond B Biol Sci.* 2019;374:20180227.

105. Gachet Y, Tournier S, Millar JB, Hyams JS. A MAP kinase-dependent actin checkpoint ensures proper spindle orientation in fission yeast. *Nature.* 2001;412:352-355.

106. Heng YW, Koh CG. Actin cytoskeleton dynamics and the cell division cycle. *Int J Biochem Cell Biol.* 2010;42:1622-1633.

107. Lee K, Song K. Actin dysfunction activates ERK1/2 and delays entry into mitosis in mammalian cells. *Cell Cycle.* 2007;6:1487-1495.

108. Rupes I, Webb BA, Mak A, Young PG. G2/M arrest caused by actin disruption is a manifestation of the cell size checkpoint in fission yeast. *Mol Biol Cell.* 2001;12:3892-3903.

109. Shrestha D, Choi D, Song K. Actin Dysfunction Induces Cell Cycle Delay at G2/M with Sustained ERK and RSK Activation in IMR-90 Normal Human Fibroblasts. *Mol Cells.* 2018;41:436-443.

110. Yan Y, Black CP, Cowan KH. Irradiation-induced G2/M checkpoint response requires ERK1/2 activation. *Oncogene.* 2007;26:4689-4698.

111. Yan Y, Hein AL, Greer PM, Wang Z, Kolb RH, Batra SK, Cowan KH. A novel function of HER2/Neu in the activation of G2/M checkpoint in response to gamma-irradiation. *Oncogene.* 2015;34:2215-2226.

112. Lin Z, von Gise A, Zhou P, Gu F, Ma Q, Jiang J, Yau AL, Buck JN, Gouin KA, van Gorp PR, Zhou B, Chen J, Seidman JG, Wang DZ, Pu WT. Cardiac-specific YAP activation improves cardiac function and survival in an experimental murine MI model. *Circ Res.* 2014;115:354-363.

113. von Gise A, Pu WT. Endocardial and epicardial epithelial to mesenchymal transitions in heart development and disease. *Circ Res.* 2012;110:1628-1645.

114. Morikawa Y, Zhang M, Heallen T, Leach J, Tao G, Xiao Y, Bai Y, Li W, Willerson JT, Martin JF. Actin cytoskeletal remodeling with protrusion

formation is essential for heart regeneration in Hippo-deficient mice. *Sci Signal.* 2015;8:ra41.

115. Kodo K, Ong SG, Jahanbani F, Termglinchan V, Hirono K, InanlooRahatloo K, Ebert AD, Shukla P, Abilez OJ, Churko JM, Karakikes I, Jung G, Ichida F, Wu SM, Snyder MP, Bernstein D, Wu JC. iPSC-derived cardiomyocytes reveal abnormal TGF-beta signalling in left ventricular non-compaction cardiomyopathy. *Nat Cell Biol.* 2016;18:1031-1042.

116. D'Amato G, Luxan G, del Monte-Nieto G, Martinez-Poveda B, Torroja C, Walter W, Bochter MS, Benedito R, Cole S, Martinez F, Hadjantonakis AK, Uemura A, Jimenez-Borreguero LJ, de la Pompa JL. Sequential Notch activation regulates ventricular chamber development. *Nat Cell Biol.* 2016;18:7-20.

117. Luxan G, Casanova JC, Martinez-Poveda B, Prados B, D'Amato G, MacGrogan D, Gonzalez-Rajal A, Dobarro D, Torroja C, Martinez F, Izquierdo-Garcia JL, Fernandez-Friera L, Sabater-Molina M, Kong YY, Pizarro G, Ibanez B, Medrano C, Garcia-Pavia P, Gimeno JR, Monserrat L, Jimenez-Borreguero LJ, de la Pompa JL. Mutations in the NOTCH pathway regulator MIB1 cause left ventricular noncompaction cardiomyopathy. *Nat Med.* 2013;19:193-201.

118. Faber JW, D'Silva A, Christoffels VM, Jensen B. Lack of morphometric evidence for ventricular compaction in humans. *J Cardiol.* 2021;78:397-405.